Tire Model Verification and Performance Comparison using Double Lane Change Test

Mohd Azman Abdullah[1*], Mohd Hanif Harun[1], Fauzi Ahmad[1], Amrik Singh Phuman Singh[1], Ahmed Esmael Mohan[2]

[1] Centre for Advanced Research on Energy (CARe), Fakulti Kejuruteraan Mekanikal (Faculty of Mechanical Engineering), Universiti Teknikal Malaysia Melaka, 75450 Ayer Keroh, Melaka, Malaysia
[2] Al-Furat Al-Awsat Technical University, Technical College Al-Mussaib, 54003 Babylon, Iraq

ABSTRACT

Three tire models, namely Dugoff, Calspan, and Magic Formula are used in this paper. The models are developed based on their equations in Matlab/Simulink and verified using CarSim software through the standard double lane change (DLC) test. The comparison of their performances is carried out on three different vehicles namely the sedan, the sports car, and the sport utility vehicle (SUV) and at three different speeds. Further analyses are performed on the lateral and longitudinal tire forces performances of the vehicles at different speeds on the DLC test. It can be observed that the DLC test is best carried out at low speed and with a less heavy vehicle. The tire models can be used for future analysis of vehicle lateral and longitudinal dynamics.

KEYWORDS: *Double lane change, tire models, vehicle dynamics, tire dynamics, tire model verification.*

1.0   INTRODUCTION

The vehicle dynamic can be modelled and simulated for the purpose of study and analysis. Vehicle dynamics are concerned with the movements of vehicles, which including acceleration, braking, ride, and cornering. The dynamic behaviour, which is determined by the forces imposed on the vehicle from the tires, gravity, and aerodynamics also can observe through simulation [1-17]. These methods are used in analyzing and studying the dynamics performances of vehicles due to the constraints such as cost, time, and safety of other approaches. The vehicle dynamics system interaction consists of the input by visual (from the driver camera), ground elevations and surface irregularities which act on the tires and aerodynamic loads which act on the body of the vehicle. The outputs evaluation of the vehicle is measured in terms of performance, handling, and ride [18-42]. The vehicle and its components are studied to determine what forces will be produced by each of these sources at a particular manoeuvre and how the vehicle will respond to these forces. Forces and moments from the road act on each tire of the vehicle and highly affected the vehicle's dynamic. The tire deforms due to the vertical load on it and makes contact with the roads over a non-zero footprint area, which is called as contact patch. Forces and moments from the road act on each tire of the vehicle and highly influence the dynamics of the vehicle. The forces acting on the tire are assumed to be at the centre of the contact patch and these forces can be composed along 3 axes (Figure 1), which are: X-axis: longitudinal tire force, F_x, Y-axis: lateral tire force, F_y, and Z-axis: normal to

vertical tire force, F_z. Besides that, the moments acting on the tire can be decomposed to 3 axes too, which are: X-axis: overturning moment, M_x, Y-axis: rolling resistance moment, M_y, and Z-axis: aligning moment, M_z. Longitudinal tire force at small slip ratio is in the forward direction in case of a driving wheel and proportional to the slip ratio, which means, longitudinal tire force at small slip ratio will increase as the slip ratio is increased. The slip ratio is the difference between theoretically calculated forward speed based on angular speed of the rim and rolling radius, and actual speed of the vehicle, expressed as a percentage of the latter. Longitudinal tire force generated by each tire depends on slip ratio, vertical forces on the tire, and friction coefficient of the road surface. The lateral tire force at a small slip angle is proportional to the slip angle. The lateral tire force at a small slip angle is increases as the slip angle is increased. The slip angle of the tire is an angle between the direction of heading and direction of travel of the wheel. In this study, the tire dynamic equations for the sedan car, sports car and SUV are modeled using Magic, Calspan and Dugoff tire formulae in Matlab/Simulink and simulated to study their performance. The models are verified through double lane change (DLC) test using commercial software CarSim.
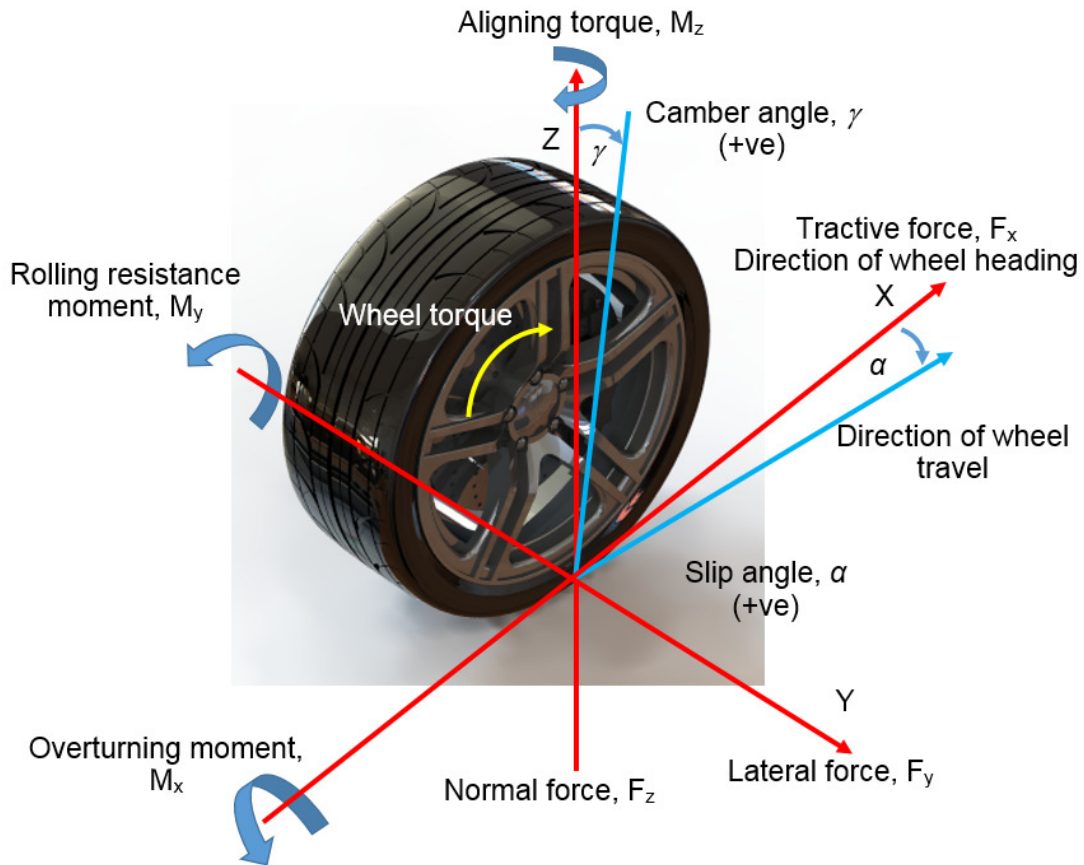

Figure 1: Tire forces and moments

In the Magic tire model, the lateral tire force derivation requires tire slip angle and the longitudinal tire force derivation requires longitudinal tire slip ratio [43-51]. The lateral tire force, F_y is calculated by,

$$F_y = D \sin(C \tan^{-1}(B\phi)) + S_v \tag{1}$$

where,

$$D = a_1 F_z^2 + a_2 F_z \tag{1}$$

$$C = 1.30 \tag{2}$$

$$B = B_1 + \Delta B_1 \tag{3}$$

$$\phi = (1 - E)(\alpha + S_h) + \frac{E}{B} \tan^{-1}\{B(\alpha + S_h)\} \tag{4}$$

and,

$$S_v = (a_{10} F_z^2 + a_{11} F_z)\gamma \tag{5}$$

The vertical tire force, F_z in Eqn(2) is the input from the simulation results in the unit of kN. The values of B_1 and ΔB_1 in Eqn(3) are calculated by,

$$B_1 = \frac{B_{CD}}{CD} \tag{6}$$

$$\Delta B_1 = -a_{12}|\gamma|B_1 \tag{7}$$

The values of E and S_h in Eqn(4) are calculated by,

$$E = a_6 F_z^2 + a_7 F_z + a_8 \tag{8}$$

$$S_h = a_9 \gamma \tag{9}$$

The tire slip angle, α in Eqn(4) is the input from the simulation results in the unit of degree. The camber angle, γ in Eqn(5) is in the input in the unit of degree. The value B_{CD} in Eqn(6) is calculated by,

$$B_{CD} = a_3 \sin\{a_4 \tan^{-1}(a_5 F_z)\} \tag{10}$$

The longitudinal tire force, F_x is calculated by,

$$F_x = D \sin(C \tan^{-1}(B\phi)) \tag{11}$$

where $C = 1.65$ and D is the same as in Eqn(2). The value B and ϕ are calculated by,

$$B = \frac{B_{CD}}{CD} \tag{12}$$

$$\phi = (1 - E)\sigma + \frac{E}{B} \tan^{-1}(B\sigma) \tag{13}$$

The value B_{CD} in Eqn(12) is calculated by,

$$B_{CD} = \frac{a_3 F_z^2 + a_4 F_z}{e^{a_5 F_z}} \tag{14}$$

The longitudinal tire slip ratio, σ in Eqn(13) is the input from the simulation results. The value E in Eqn(13) is calculated by,

$$E = a_6 F_z^2 + a_7 F_z + a_8 \tag{15}$$

The constants a_1, a_2, a_3, a_4, a_5, a_6, a_7, a_8, a_9, a_{10}, a_{11}, a_{12} and a_{13} are tabulated in Table 1 and 2 [45, 48, 49, 51].

Table 1: Constants a_1 to a_8

Force	a_1	a_2	a_3	a_4	a_5	a_6	a_7	a_8
F_y	-22.1	1011	1078	1.82	0.208	0.000	-0.354	0.707
F_x	-21.3	1144	49.6	226	0.069	-0.006	0.056	0.486

Table 2: Constants a_9 to a_{13}

Force	a_9	a_{10}	a_{11}	a_{12}	a_{13}
F_y	0.028	0.000	14.8	0.022	0.000

In Calspan tire model, the lateral and longitudinal tire forces are derived from the combination of tire slip conditions [52-60]. The lateral and longitudinal tire forces, F_y and F_x are calculated by,

$$F_y = \frac{f(\sigma) C_\alpha \tan \alpha}{\sqrt{C_\alpha^2 \tan^2 \alpha + C_{\sigma_x}'^2 \sigma_x^2}} \mu F_z \tag{16}$$

$$F_x = \frac{f(\sigma) C_{\sigma_x}' \sigma_x}{\sqrt{C_\alpha^2 \tan^2 \alpha + C_{\sigma_x}'^2 \sigma_x^2}} \mu F_z \tag{17}$$

where,

$$f(\sigma) = \frac{F_c}{\mu F_z} = \frac{C_1 \sigma^3 + C_2 \sigma^2 + \left(\frac{4}{\pi}\right) \sigma}{C_1 \sigma^3 + C_3 \sigma^2 + C_4 \sigma + 1} \tag{18}$$

$$C_{\sigma_x}' = C_{\sigma_x} + \left(C_\alpha - C_{\sigma_x}\right) \sqrt{\sin^2 \alpha + \sigma_x^2 \cos^2 \alpha} \tag{19}$$

$$\mu = \mu_o + \left(1 - K_\mu \sqrt{\sin^2 \alpha + \sigma_x^2 \cos^2 \alpha}\right) \tag{20}$$

The lateral and longitudinal tire stiffnesses, C_α and $C_{\sigma x}$, in Eqn(16) and Eqn(19) are calculated by,

$$C_\alpha = \frac{2}{(a_{po})^2}\left(A_o + A_1 F_z - \frac{A_1}{A_2}F_z^2\right) \tag{21}$$

$$C_{\sigma_x} = \frac{2}{(a_{po})^2}F_z(CS/FZ) \tag{22}$$

The values of tire slip angle, α, vertical tire force, F_z, and longitudinal slip ratio, σ_x are the inputs from the simulation results. The combined slip, σ in Eqn(18) is calculated by,

$$\sigma = \frac{\pi a_p^2}{8\mu_o F_z}\sqrt{C_\alpha^2 \tan^2 \alpha + C_{\sigma_x}^2\left(\frac{\sigma_x}{1-\sigma_x}\right)^2} \tag{23}$$

The original contact length, a_{po}, in Eqn(21) and Eqn(22) is calculated by,

$$a_{po} = \frac{0.0768\sqrt{F_z F_{ZT}}}{T_w(T_p + 5)} \tag{24}$$

The value of tire contact patch, a_p, in Eqn(23) is calculated by,

$$a_p = a_{po}\left(1 - K_a \frac{F_x}{F_z}\right) \tag{25}$$

All the constants in Eqn(18) and Eqn(20) to (25) are tabulated in Table 3 [99].

Table 3: Constant for Calspan tire model

Parameters	RWD radial	RWD bias ply	FWD radial	FWD radial
Tire Designation	155SR13	P155/80D13	P185/70 R13	P185/70 R13
Thread Width, T_w	6	6	7.3	7.3
Tire Pressure, T_p	24	24	24	24
FZT	810	900	980	980
C_1	1.0	0.535	1.0	1.0
C_2	0.34	1.05	0.34	0.34
C_3	0.57	1.15	0.57	0.57
C_4	0.32	0.8	0.32	0.32
A_0	914.02	1817	1068	1068
A_1	12.9	7.48	11.3	11.3
A_2	2028.24	2455	2442.73	2442.73
A_3	1.19	1.857	0.31	0.31
K_4	0.05	0.2	0.05	0.05
CS/FZ	18.7	15.22	17.91	17.91
μ_o	0.85	0.85	0.85	0.85

In Dugoff tire model, the lateral and longitudinal tire forces are derived from lateral and longitudinal tire stiffness values [61-73]. The lateral and longitudinal tire forces, F_y and F_x are calculated by,

$$F_y = C_\alpha \left(\frac{\tan \alpha}{1 + \sigma_x} \right) f(\lambda) \tag{26}$$

$$F_x = C_\sigma \left(\frac{\sigma_x}{1 + \sigma_x} \right) f(\lambda) \tag{27}$$

where,

$$\lambda = \frac{\mu F_z (1 + \sigma_x)}{2 \left(\sqrt[2]{(C_\sigma \sigma)^2 + (C_\alpha \tan \alpha)^2} \right)} \tag{28}$$

$$f(\lambda) = \begin{cases} (2 - \lambda)\lambda & if \ \lambda < 1 \\ \\ 1 & if \ \lambda \geq 1 \end{cases} \tag{29}$$

The tire slip angle, α, tire longitudinal slip ratio, σ_x and tire vertical force, F_z are the inputs from simulation results. The constants in Eqn(26) to (28) are tabulated in Table 4 [61, 62, 64, 65, 66, 67, 70].

Table 4: Dugoff tire constants

Parameters	Value
C_α	-1.56 x 10^5
C_σ	2.37 x 10^5
μ	0.99

2.0   METHODOLOGY

Three different vehicles namely the sedan car, the sports car and the sport utility vehicle (SUV) are used in the simulation of DLC (Figure 2). The test is carried out at 3 different speeds of 80, 100, and 120 km/h. Figure 3 shows the standard dimension of the DLC route [74-88]. The simulation of DLC produces the vertical tire force, F_z, longitudinal tire force, F_x, lateral tire force, F_y, tire slip angle, α, and tire slip ratio, σ. The F_z, α and σ are used as the inputs for the tire models. The outputs of the tire models, F_x and F_y are compared with the F_x and F_y from the simulation. Figures 4 and 5 show the Simulink subsystem models of F_y and F_x developed from Eqn(1) and Eqn(11) respectively. Figure 6 shows the Simulink subsystem model of Calspan tire model for F_y and F_x developed from Eqn(16) and Eqn(17). Figure 7 shows the Simulink subsystem model of Dugoff tire model for F_y and F_x developed from Eqn(26) and Eqn(27). The 'miew' in Figure 7 is the constant μ in Table 4.
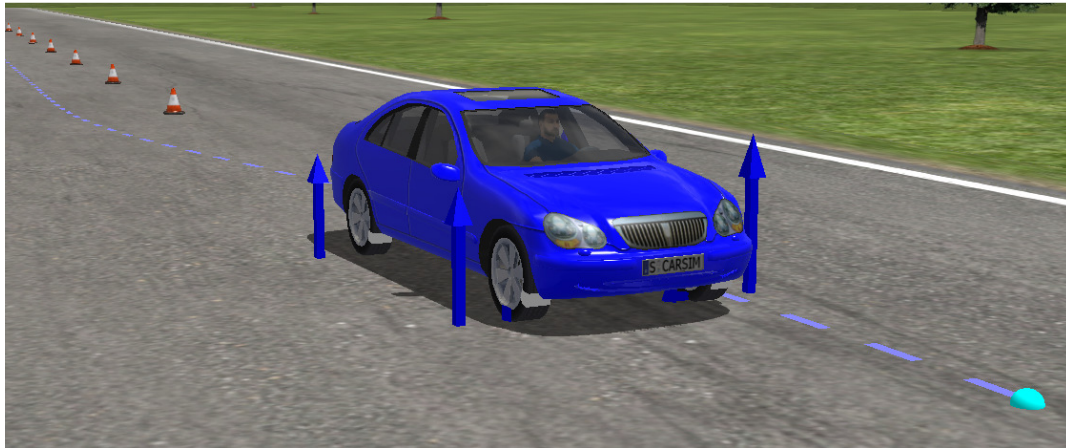
(a)

(b)

(c)

Figure 2: DLC simulation in CarSim software (a) sedan car, (b) sports car and (c) SUV
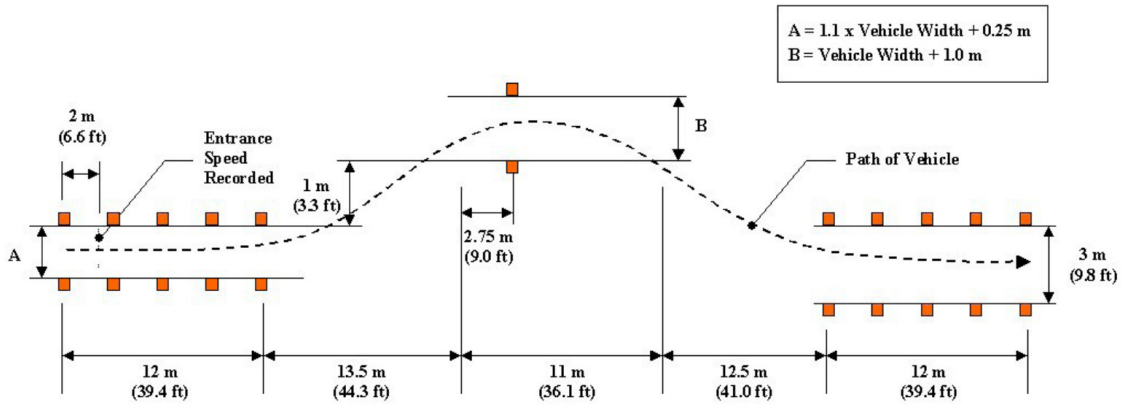
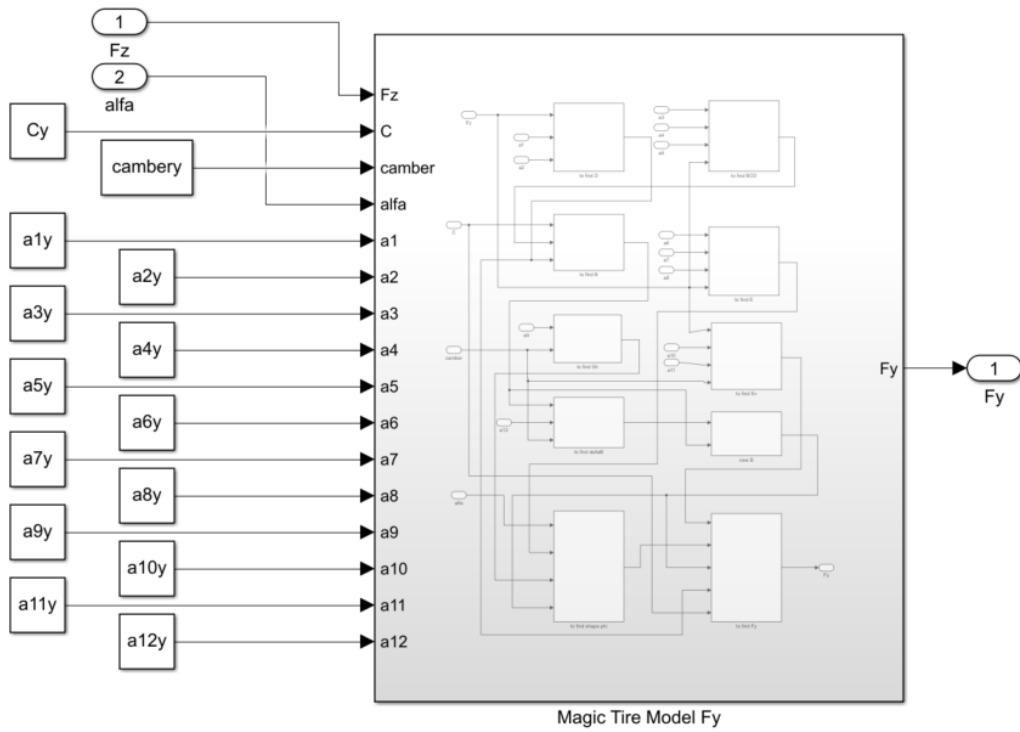Figure 3: Standard DLC procedure route (ISO 3888 Part 2)
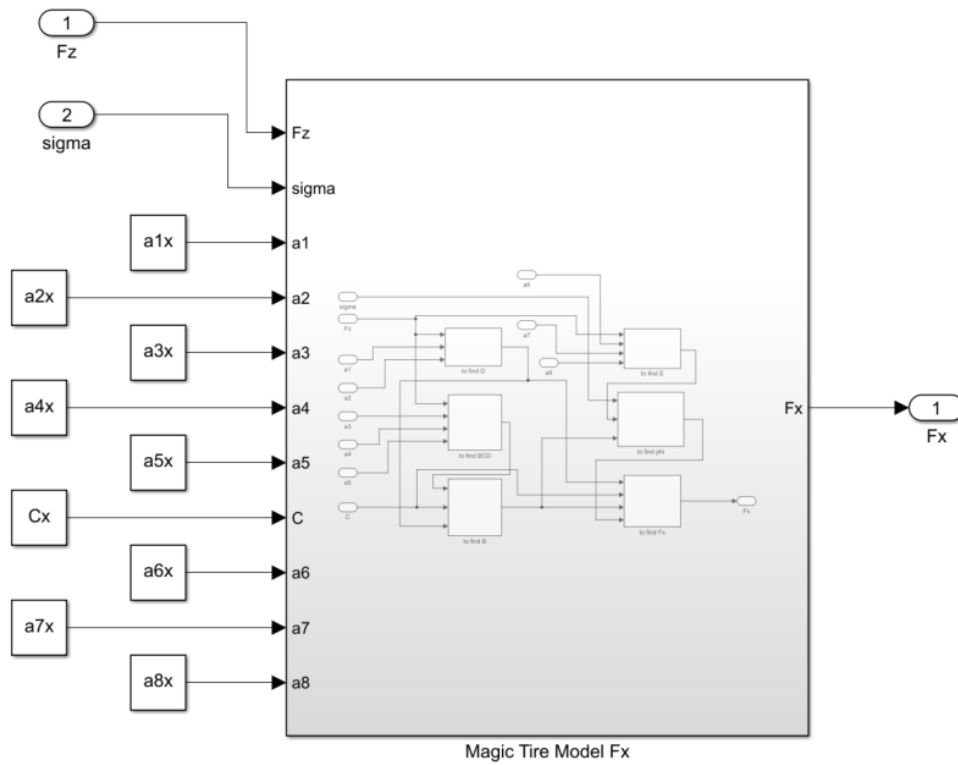

Figure 4: Magic tire Simulink model to find F_y

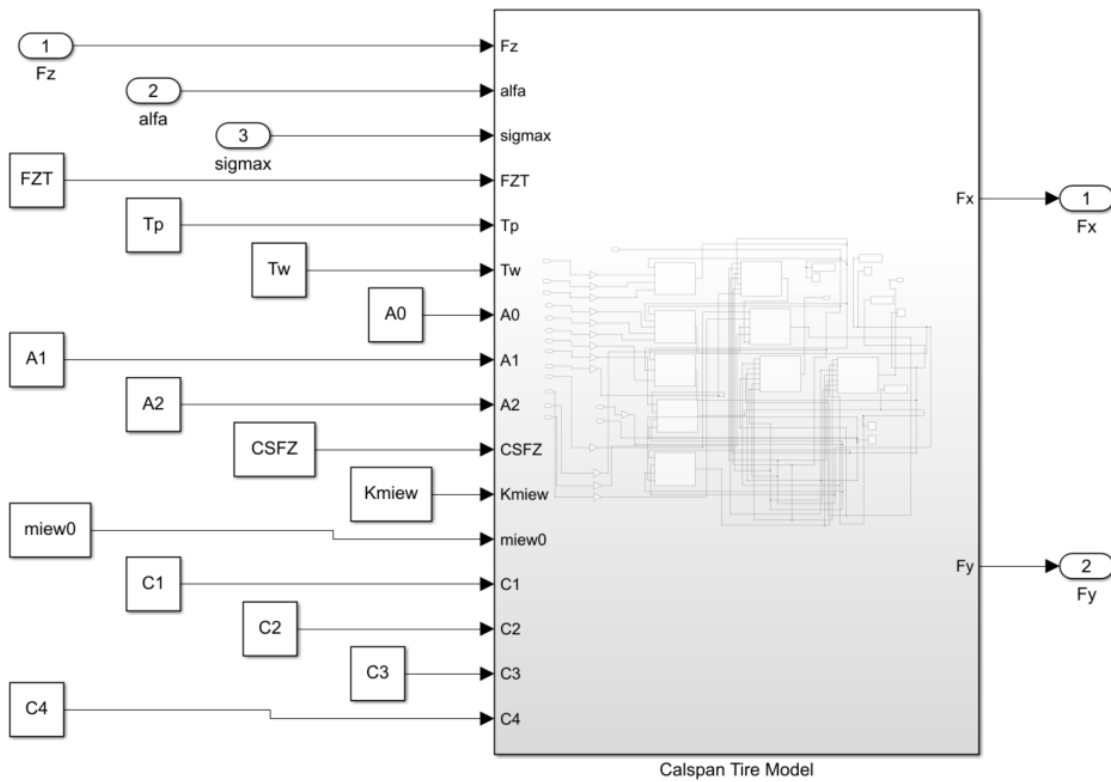Figure 5: Magic tire Simulink model to find F_x

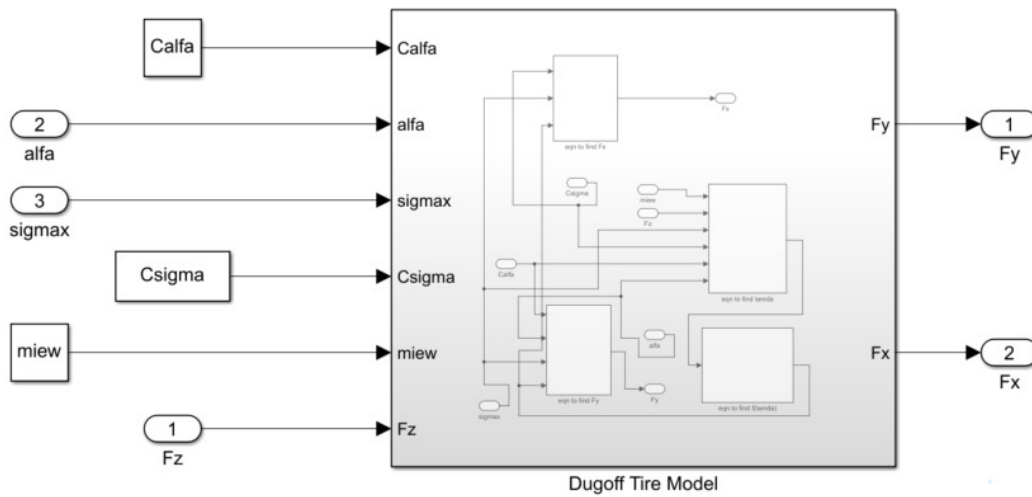Figure 6: Calspan tire Simulink model to find F_y and F_x

Figure 7: Dugoff tire Simulink model to find F_y and F_x

The verification of the models is carried through the root mean square (RMS) value of the difference between the tire forces from the model to the tire forces from the simulation. The equation of the RMS is shown in Eqn(30) with *n* is the number of data. The lower the value of RMS, the better the tire model performance. Figure 8 shows the comparison flow of the tire forces. The vertical tire force, F_z, tire slip angle, α, and tire slip ratio, σ, from the results of the simulation are used as the inputs for the model. The longitudinal and vertical tire forces from both simulation ($x_{sim,i}$) and model ($x_{model,i}$) results are compared using RMS values [89-98].

$$RMS = \sqrt{\frac{1}{n}\sum_{i=1}^{n}\left(x_{sim,i} - x_{model,i}\right)^2} \qquad (30)$$
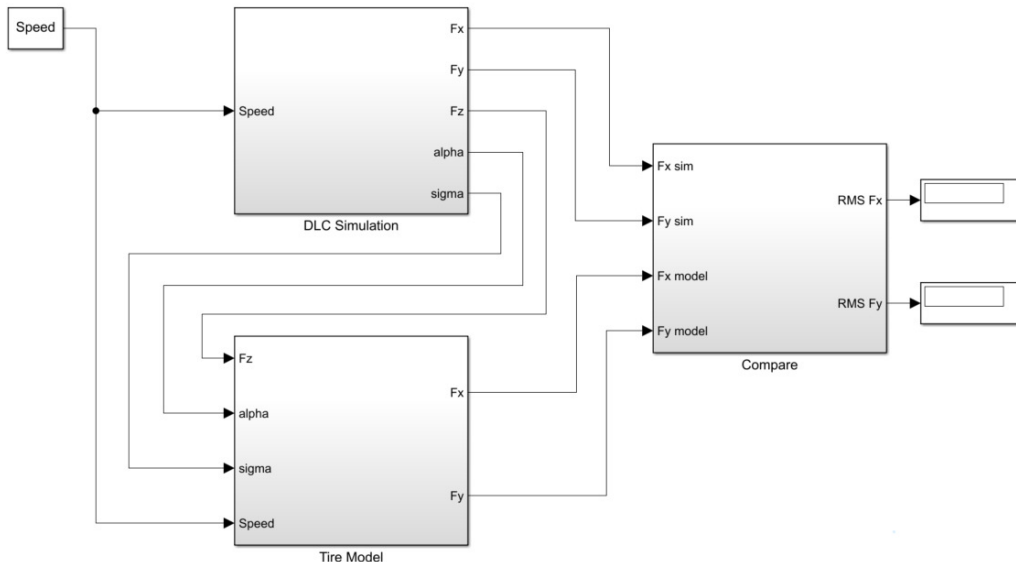

Figure 8: Comparison between simulation and model

3.0   RESULTS AND DISCUSSION

Figure 9 to 17 show the longitudinal and lateral tire forces from simulation and models for the sports car, sedan, and SUV at speeds of 80, 100, and 120 km/h DLC test. It can be observed that the shape and pattern of the graphs from the models are almost identical to the results from the simulation. At 80 km/h (Figure 9), the longitudinal and lateral tire forces from the Calspan tire model are about the same as the result from simulation for the sports car. However, only longitudinal tire forces of the Calspan tire model are about the same as in the simulation for DLC test at 100 and 120 km/h presented in Figure 10 and 11 respectively. The best graph fitting for longitudinal tire forces is from the Magic tire model at these speeds. As for the sedan type of car, at all speeds, the best tire model is Calspan where all the longitudinal and lateral tire forces are very nearly alike as the simulation as shown in Figures 12 to 14. The tire models however perform randomly for SUV (Figure 15 to 17). At 80 and 100 km/h, longitudinal tire forces from Calspan tire models are the best. But at 120 km/h, longitudinal tire force from the Magic tire model is the finest. The Magic tire model also contributes in producing the unsurpassed lateral tire force for the SUV at 80 km/h (Figure 15). At 100 and 120 km/h (Figure 16 and 17), the best tire model matching the simulation results for lateral tire forces is the Dugoff tire model.
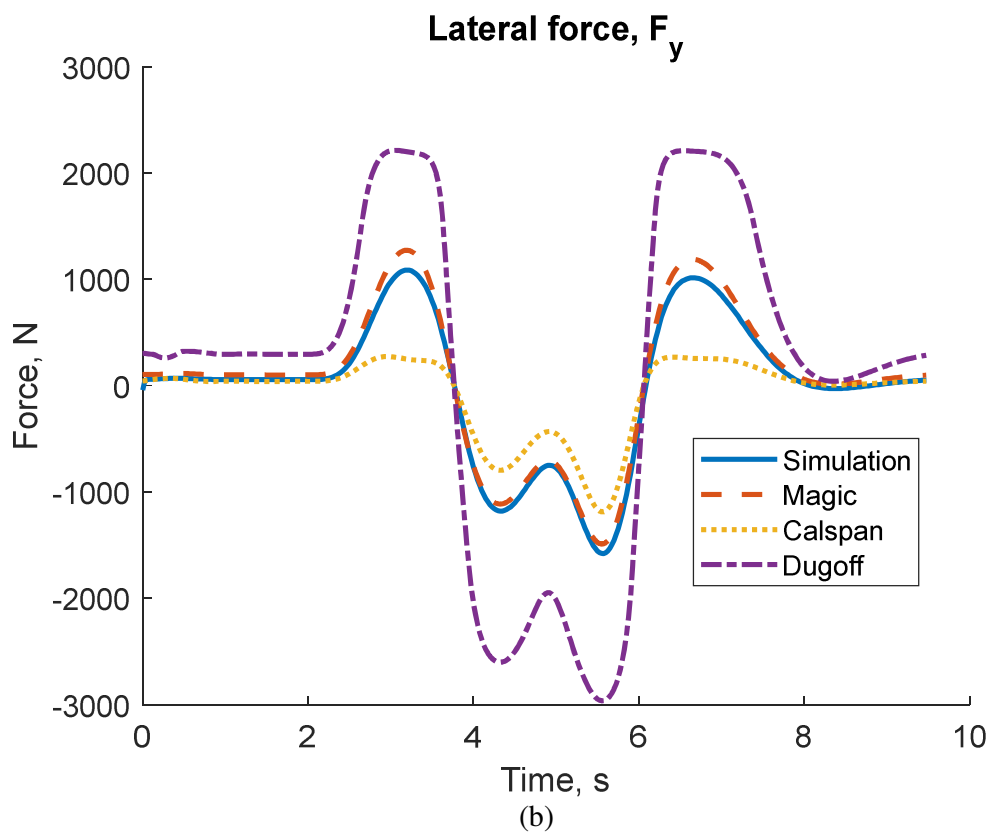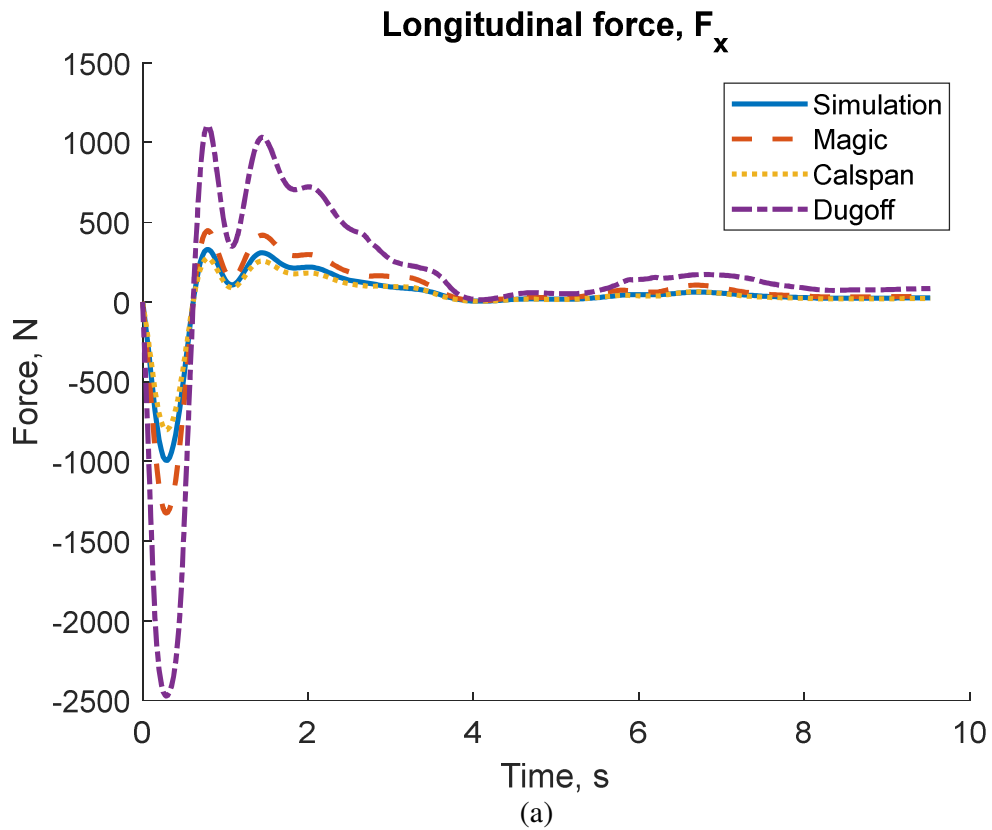
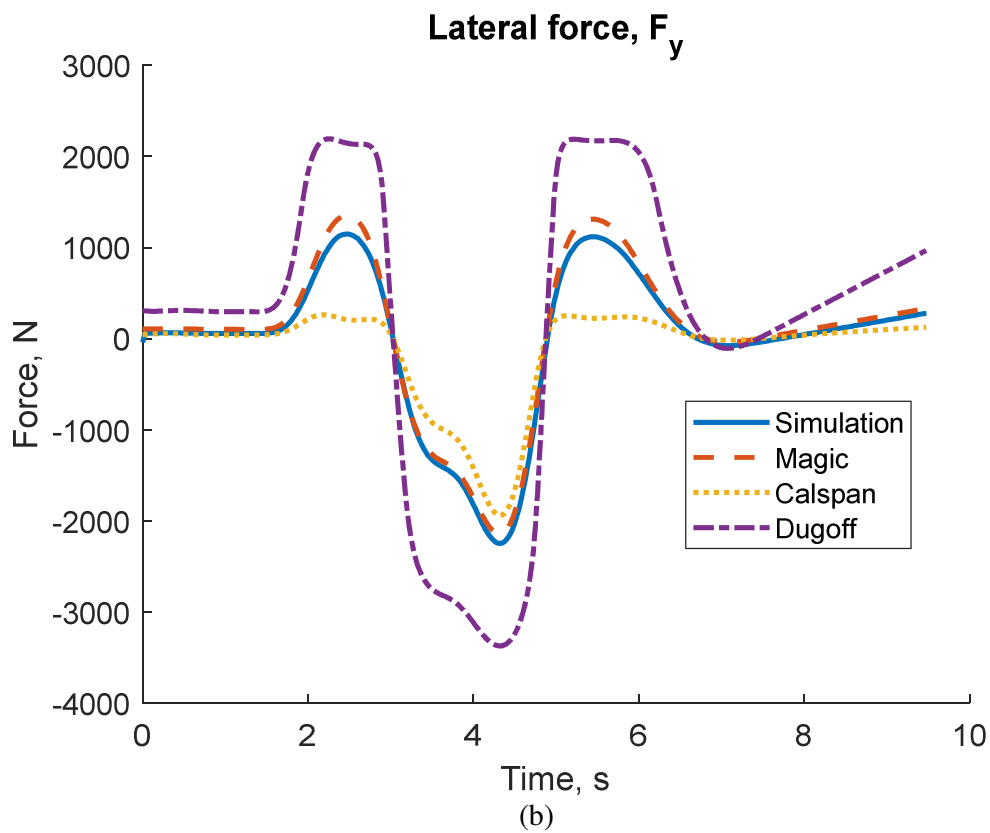Figure 9: Comparison of (a) F_x and (b) F_y for sports car at 80 km/h
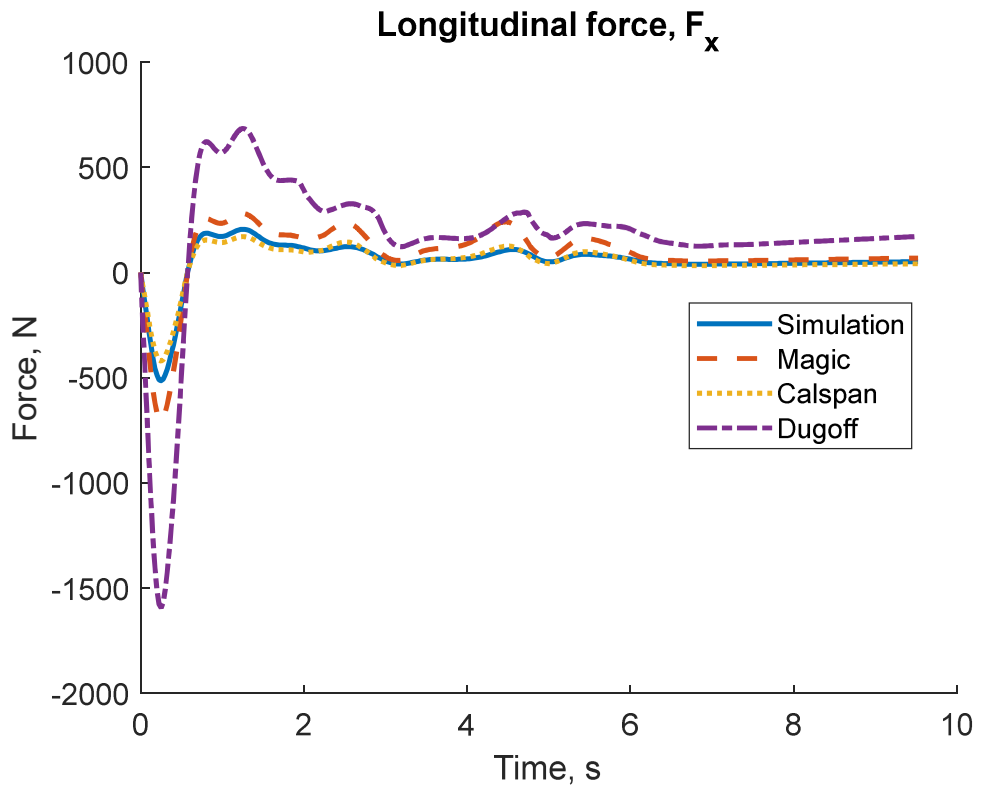
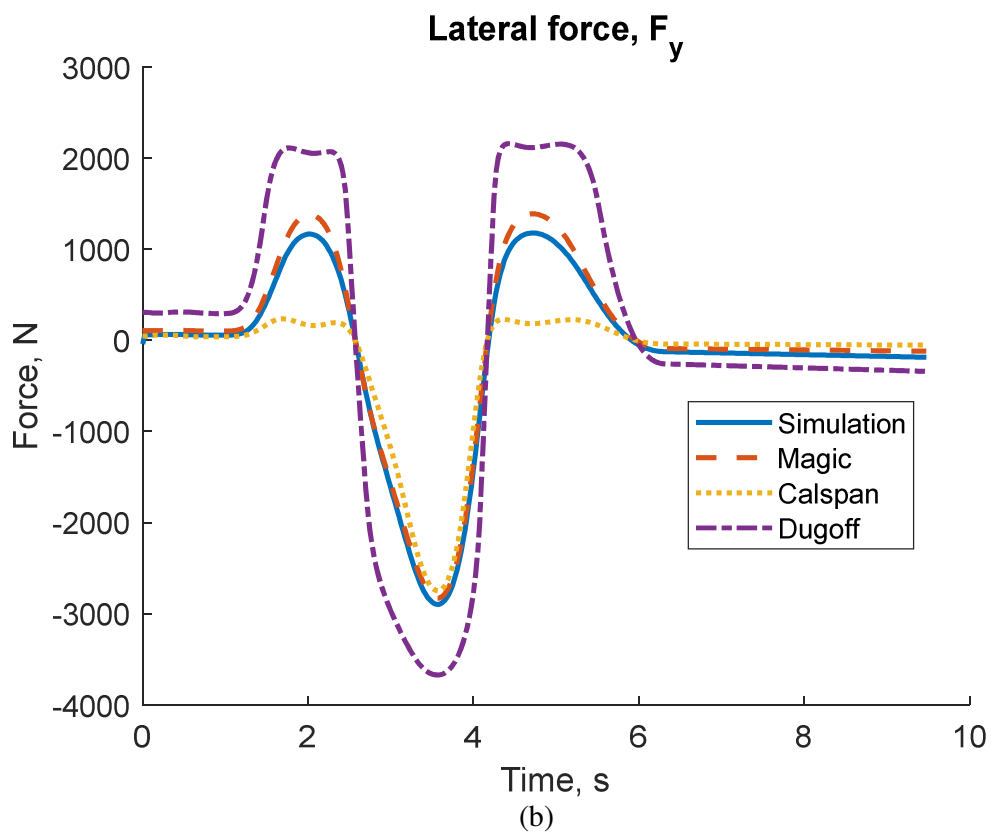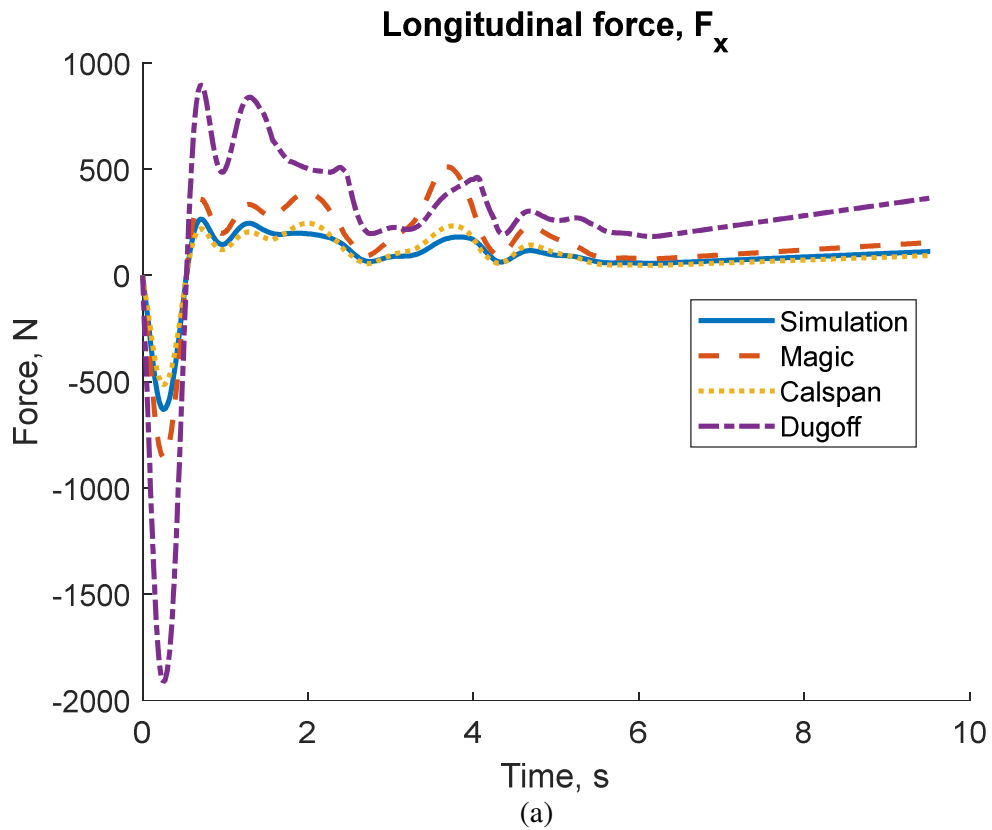Figure 10: Comparison of (a) F_x and (b) F_y for sports car at 100 km/h

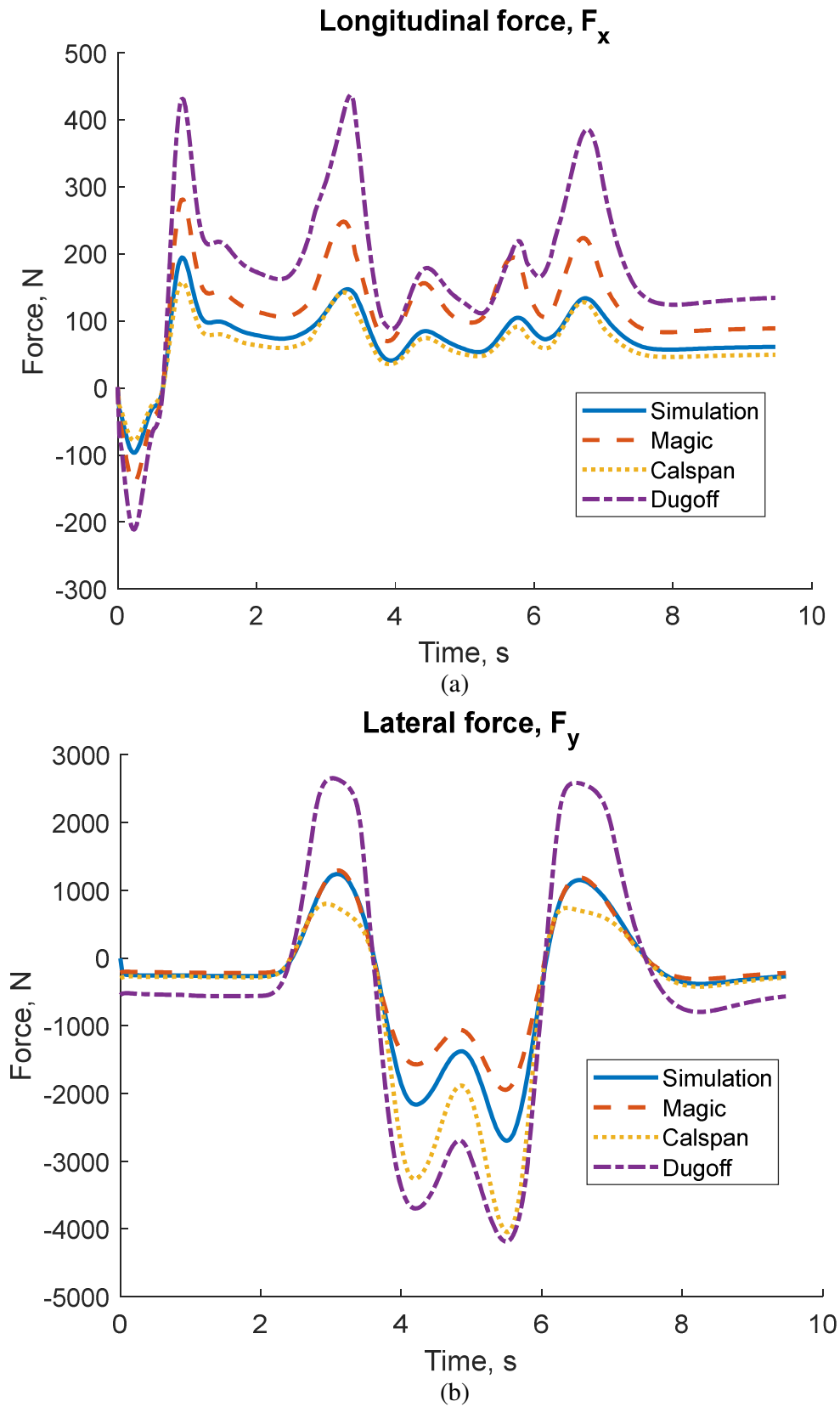Figure 11: Comparison of (a) F_x and (b) F_y for sports car at 120 km/h

(a)

(b)

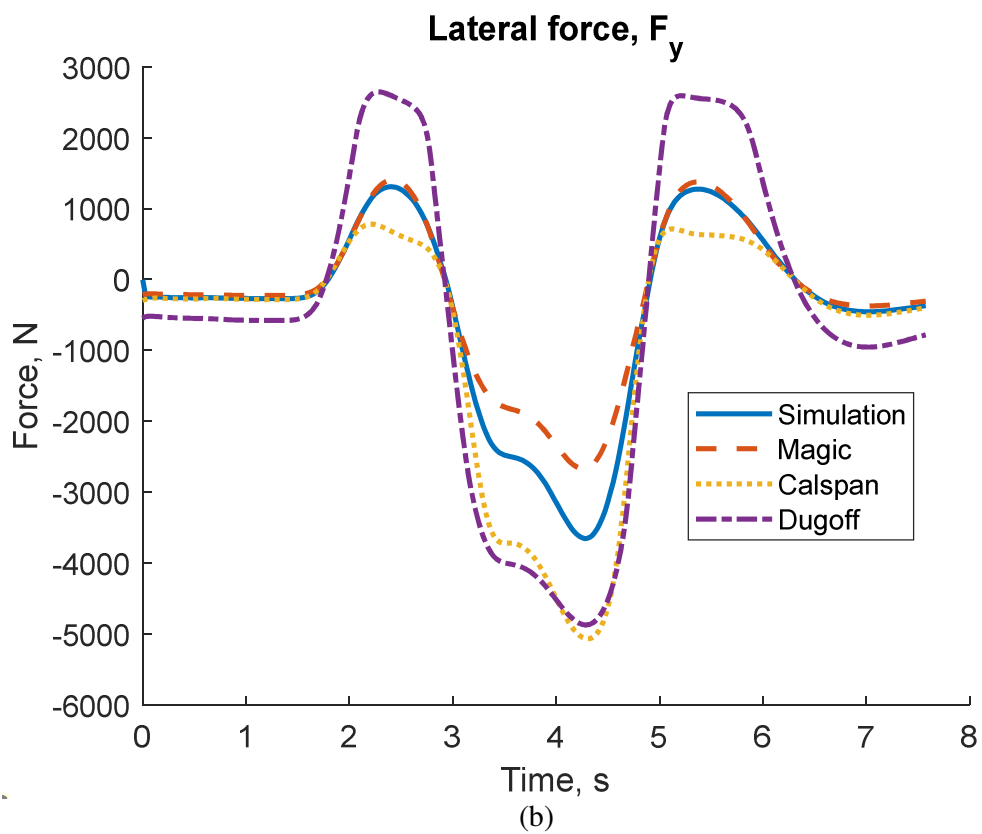Figure 12: Comparison of (a) F_x and (b) F_y for sedan car at 80 km/h
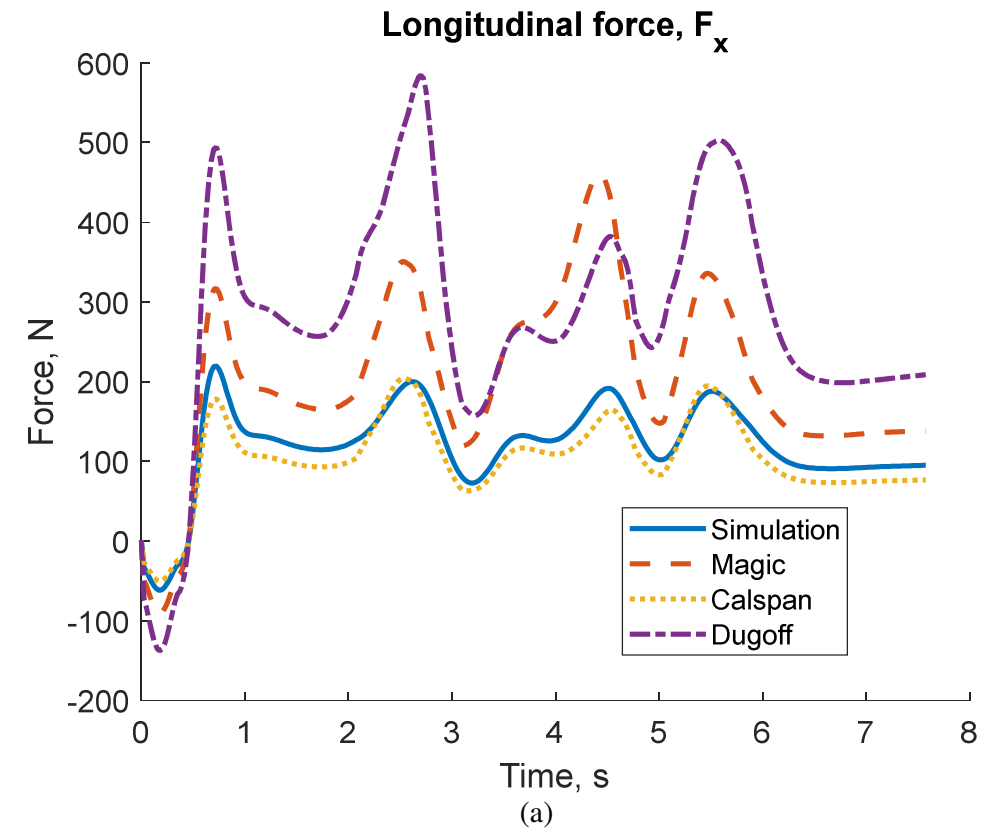
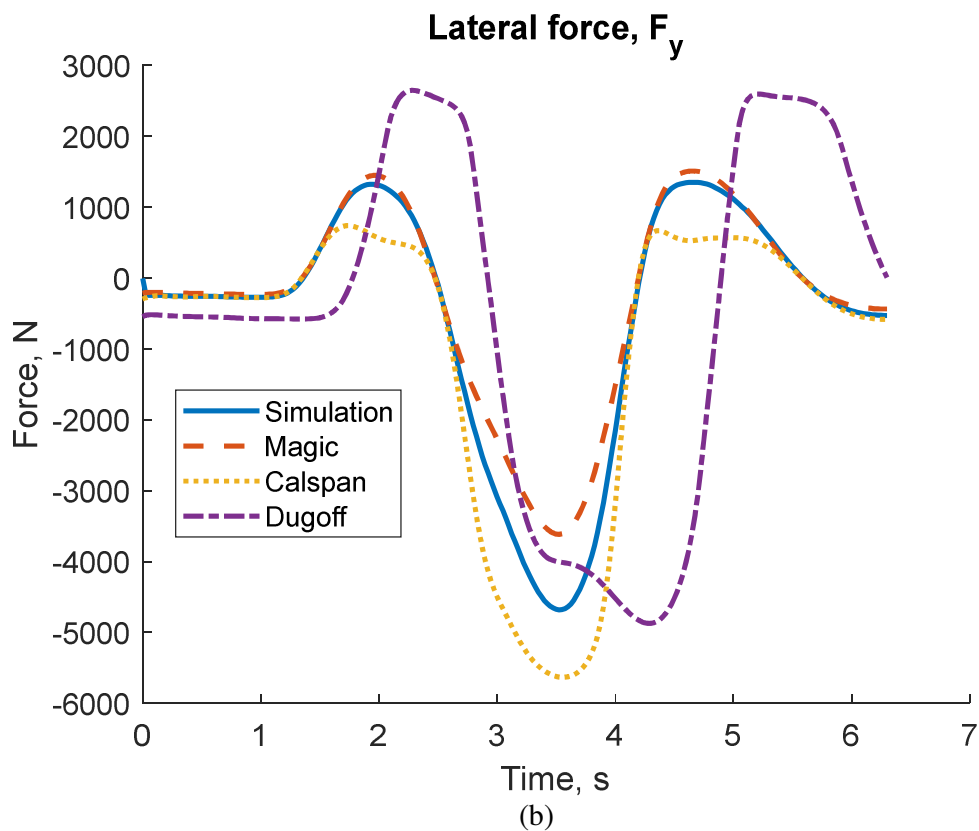Figure 13: Comparison of (a) F_x and (b) F_y for sedan car at 100 km/h
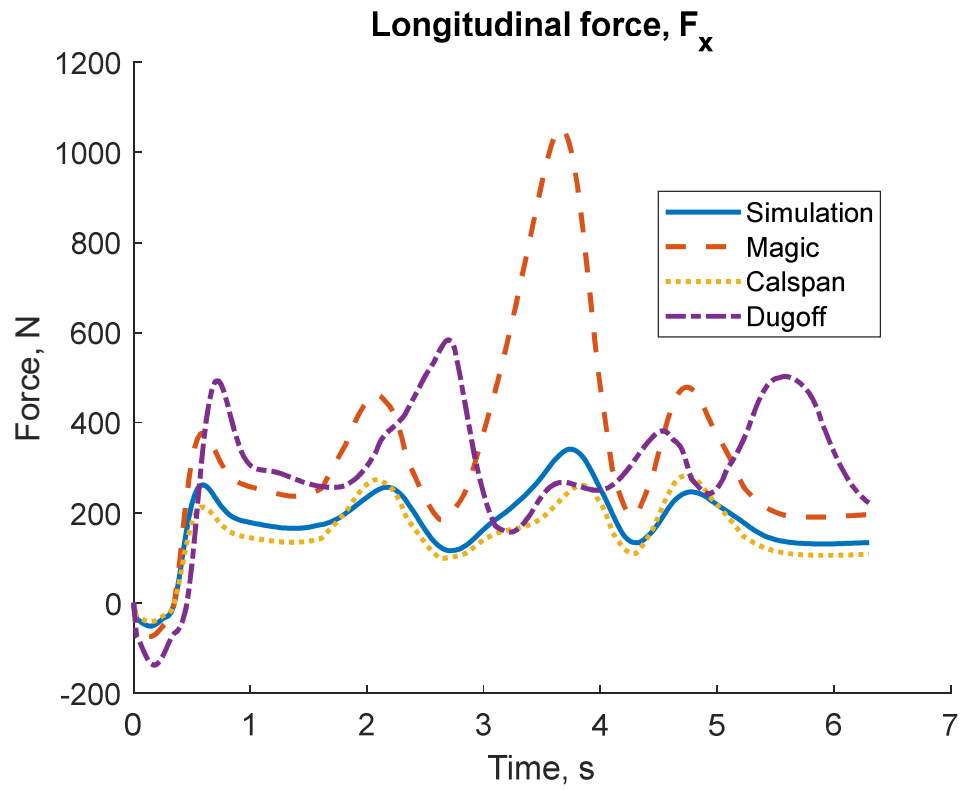
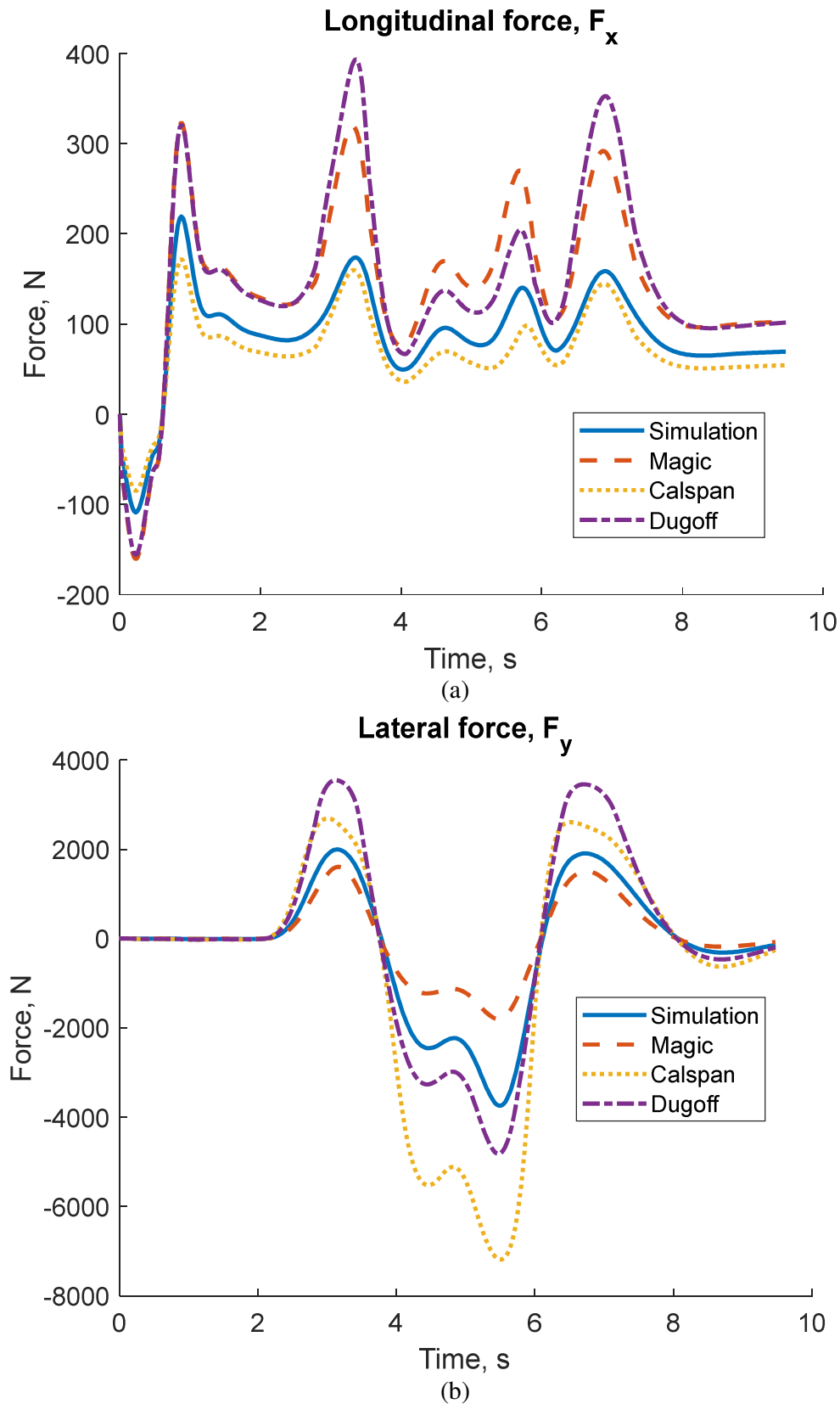Figure 14: Comparison of (a) F_x and (b) F_y for sedan car at 120 km/h

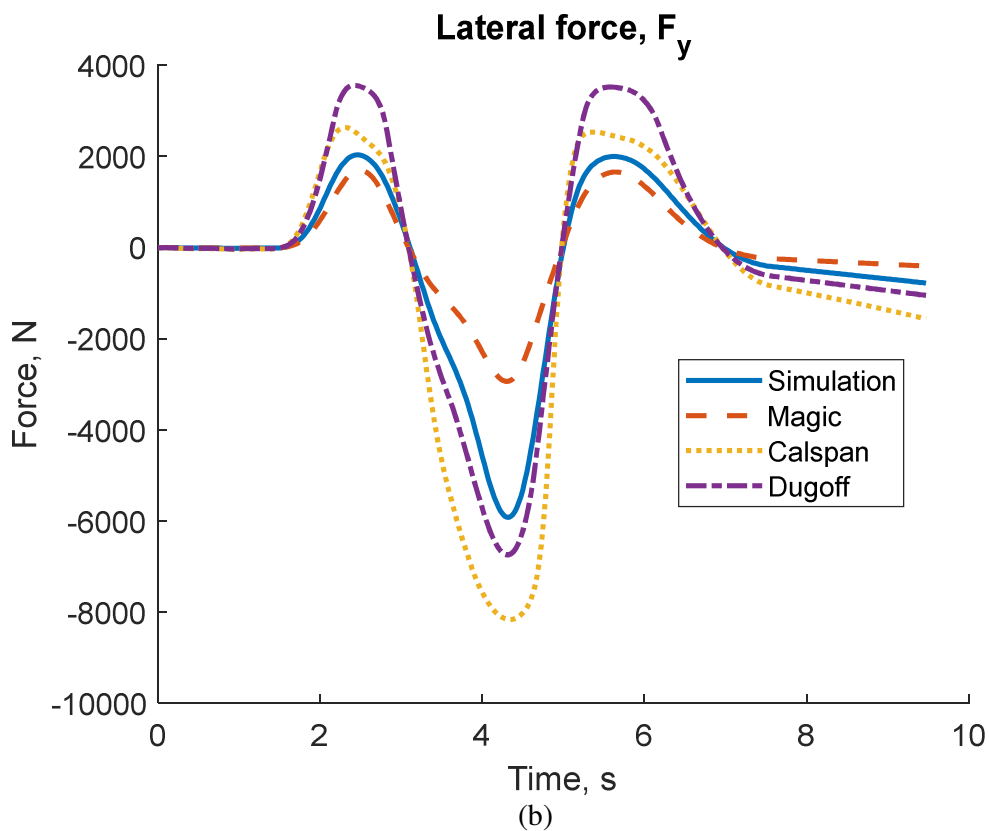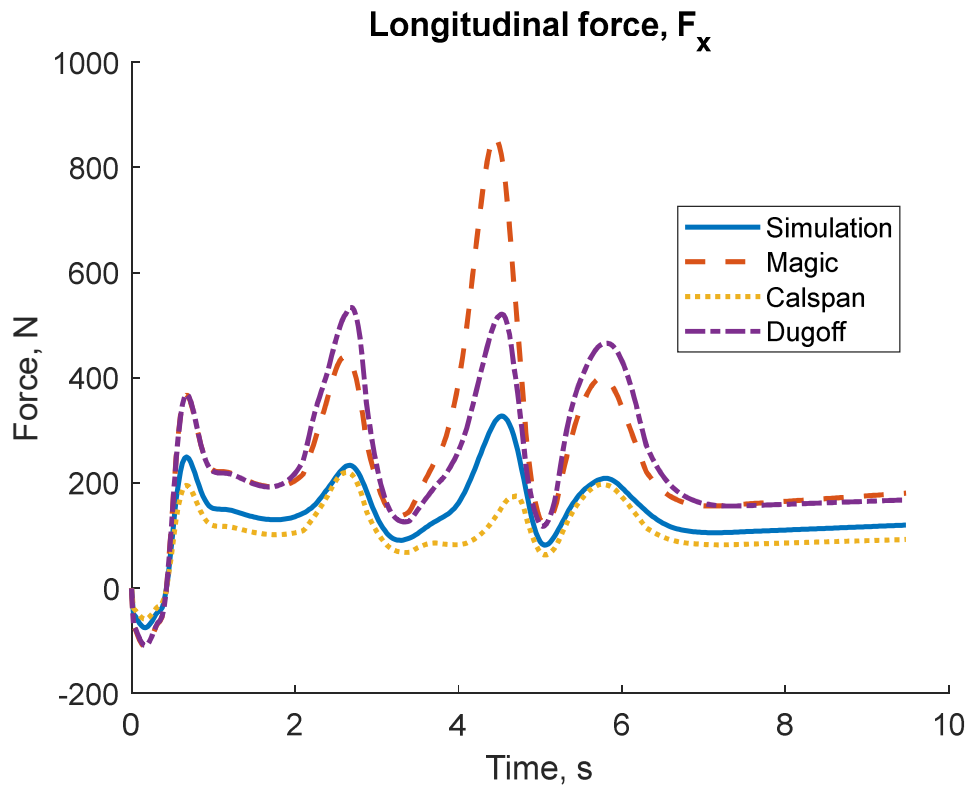Figure 15: Comparison of (a) F_x and (b) F_y for SUV at 80 km/h

Figure 16: Comparison of (a) F_x and (b) F_y for SUV at 100 km/h
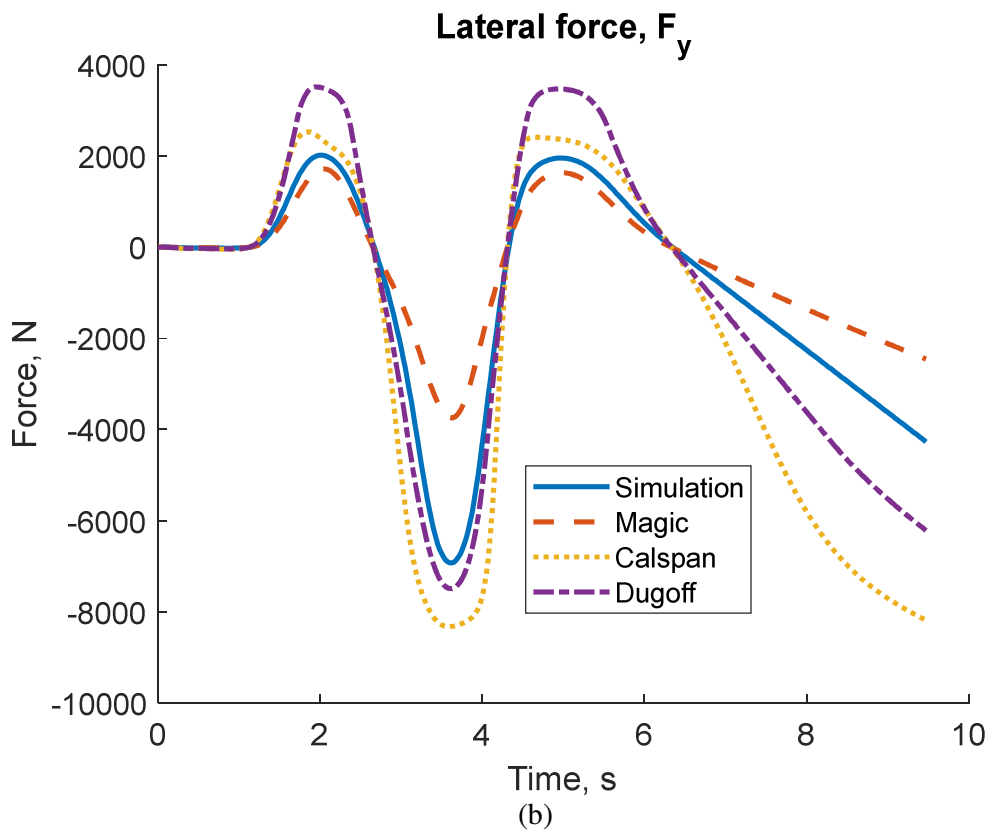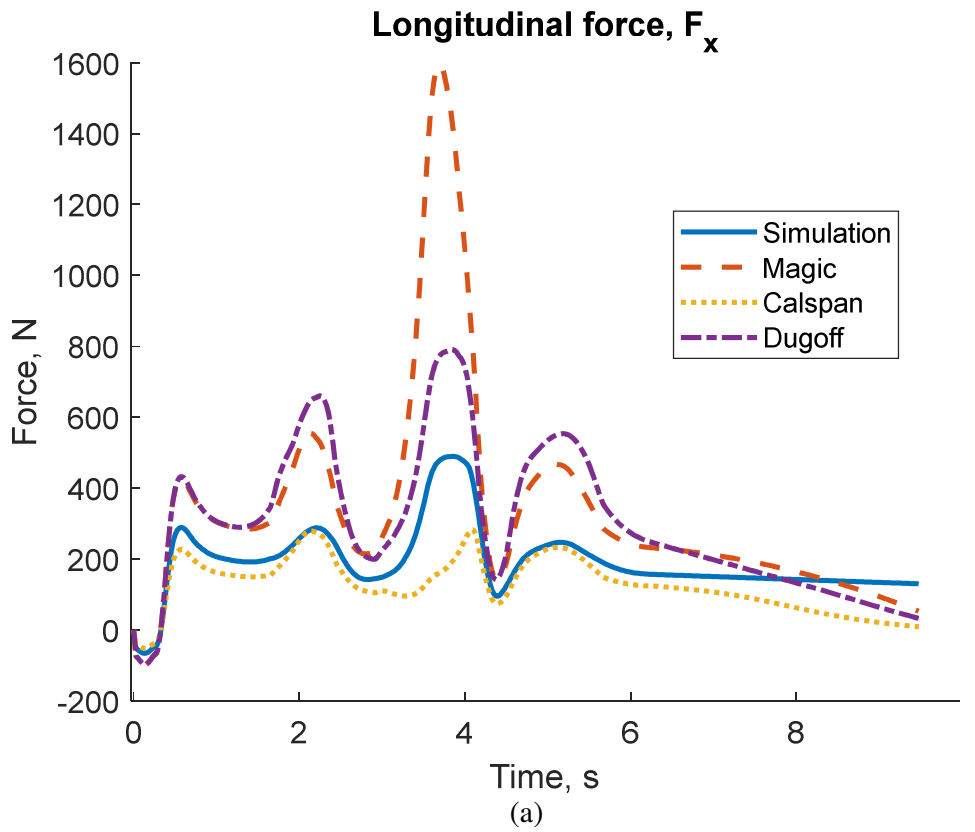
Figure 17: Comparison of (a) F_x and (b) F_y for SUV at 120 km/h

In order to verify the models, the RMS values are generated. The lower the value of RMS, the better the performance of the models. Table 5 tabulated the RMS results comparison among the tire forces from the models to the simulation. From the table, at all speeds, using the Magic tire model, the best vehicle performance is a sports car for both longitudinal and lateral tire forces. Using the Calspan tire model, the best vehicle is the sports car for longitudinal tire force and the sedan car for lateral tire force. As for the Dugoff tire model, the SUV is the best for longitudinal force and the sedan car is the best for lateral force. With average RMS of 30.03 and 80.31 for longitudinal and lateral tire forces respectively, the best speed for DLC test is at the lowest speed of 80 km/h. Comparing all tire models at all speeds, the sports car and sedan car are good using the Calspan tire model for both F_x and F_y. The SUV however is good using the Calspan tire model for F_x and Magic tire model for F_y. Among all tire models, it is observed that the Calspan tire model is the best in mimicking the result from the simulation.

Table 5: RMS values

Tire model	Speed (km/h)	80		100		120	
		RMS value					
	Vehicle type	F_x	F_y	F_x	F_y	F_x	F_y
Magic	Sport car	9.79	46.77	17.11	49.38	45.29	72.37
	Sedan	27.73	41.80	42.27	41.12	78.99	121.90
	SUV	33.63	3.21	63.07	428.30	123.80	2163.00
Calspan	Sport car	4.51	21.46	11.04	213.70	20.21	141.00
	Sedan	11.87	15.71	20.27	36.63	33.23	12.61
	SUV	15.31	31.19	28.38	905.20	125.60	3640.00
Dugoff	Sport car	59.20	273.60	126.10	856.90	269.50	158.40
	Sedan	74.41	268.70	136.80	54.40	205.50	534.60
	SUV	33.84	20.32	47.58	286.40	124.70	1919.00

Figures 18 to 20 show the simulation results from CarSim software of F_x and F_y for all vehicles at different speeds. The longitudinal forces are different among all vehicles.
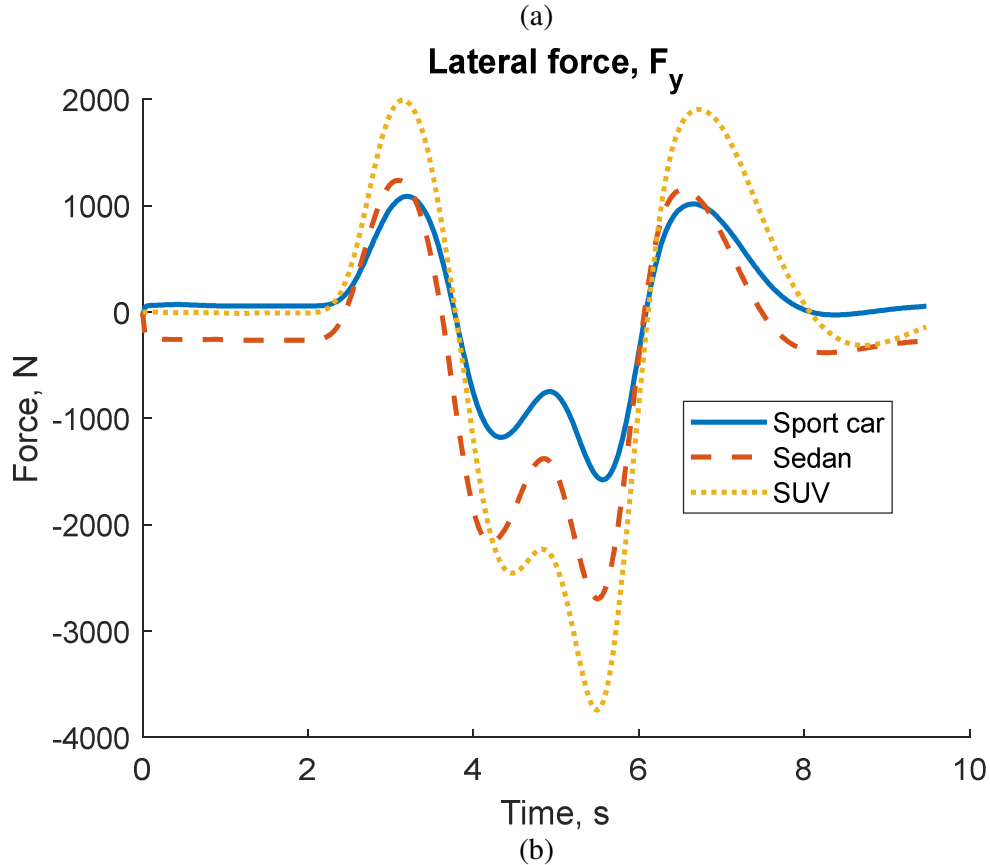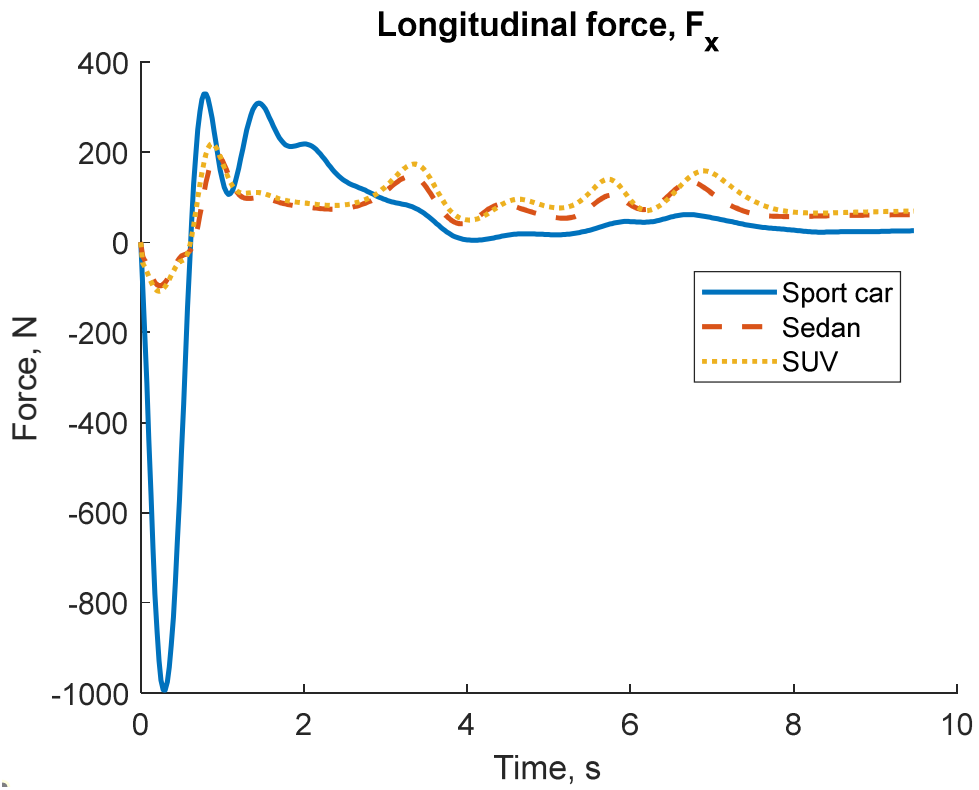
(a)

(b)

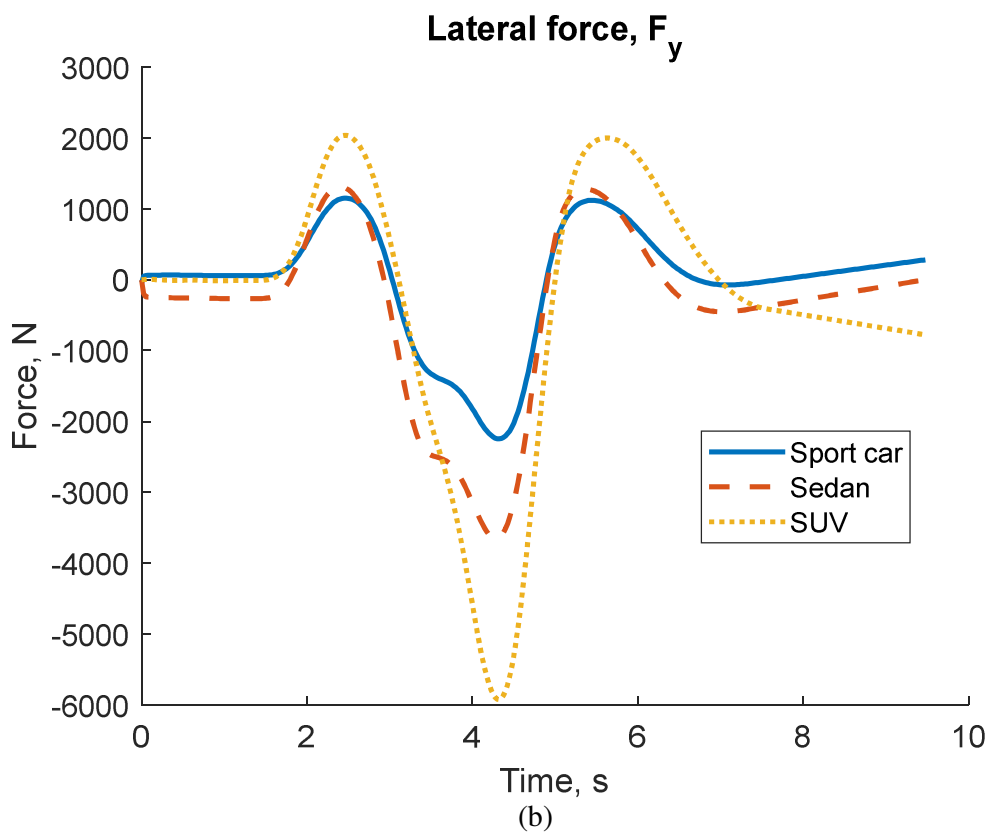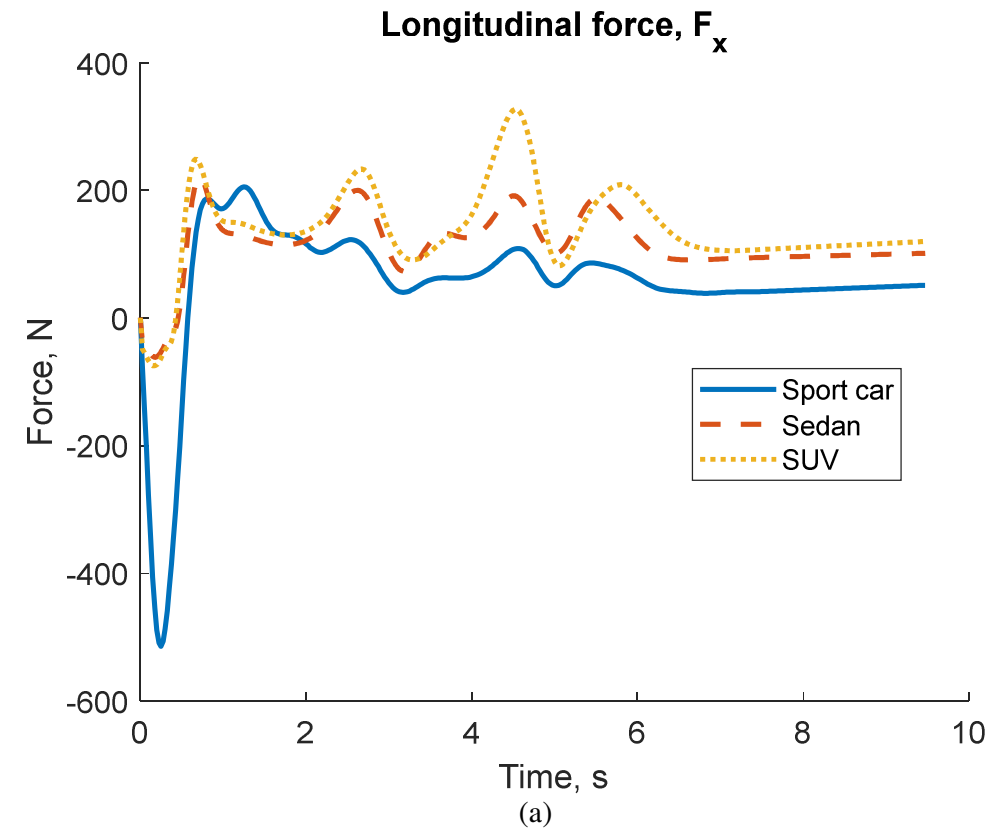Figure 18: Comparison of (a) F_x and (b) F_y for all vehicles at 80 km/h

Figure 19: Comparison of (a) F_x and (b) F_y Fy for all vehicles at 100 km/h
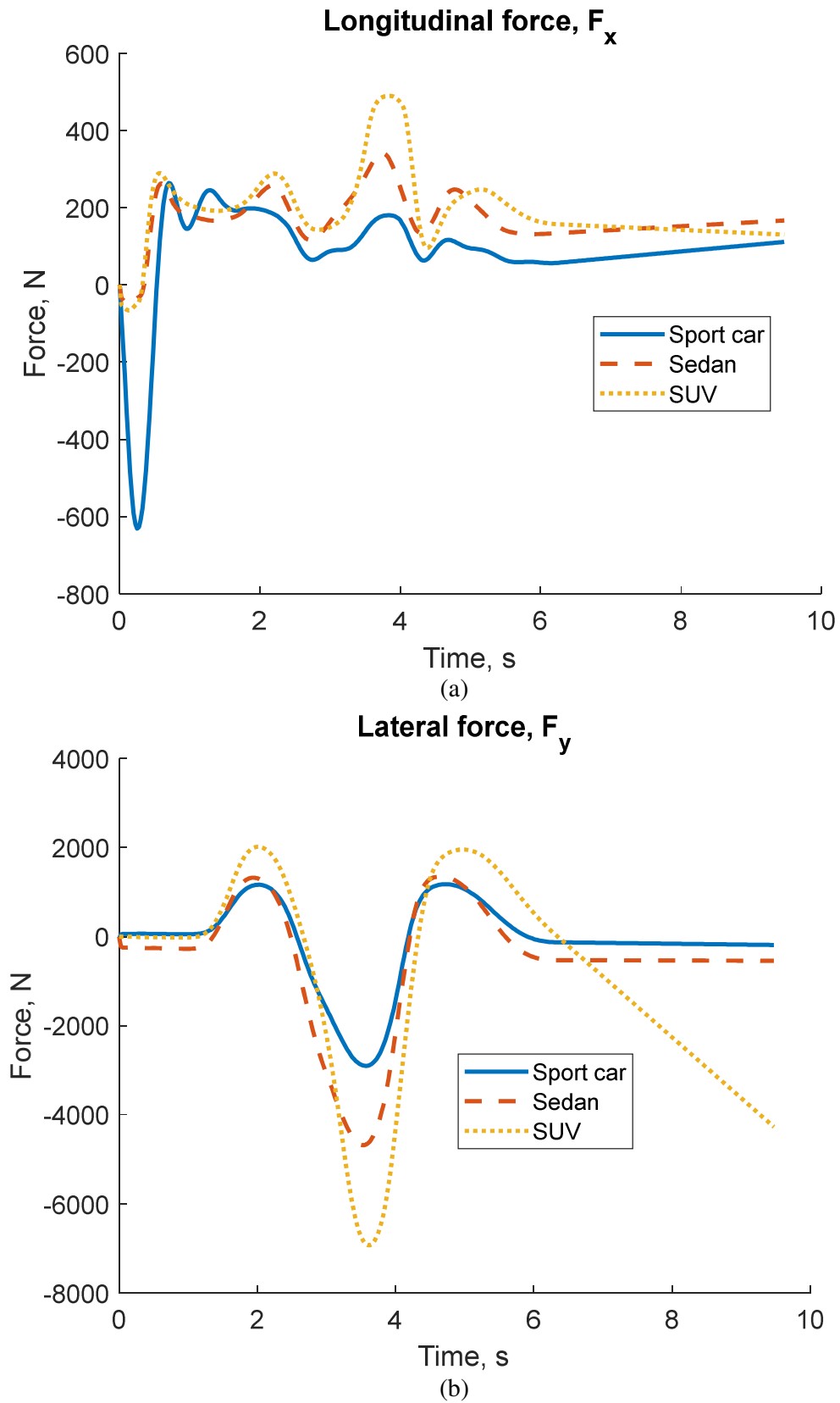
(a)

(b)

Figure 20: Comparison of (a) F_x and (b) F_y for all vehicles at 120 km/h

Figures 21 to 23 show the comparison of the *y*-coordinate of all vehicles to the targeted route. At 80 and 100 km/h, the *y*-coordinates of SUV are quite offset compared to the other vehicles. This is merely due to the lateral acceleration and lateral force. Since SUV is the heaviest vehicle, the lateral force is the highest. At zone A when the SUV arrives, due to the momentum, the vehicle tends to go further, however, the counter-steering wheel action returns the SUV to the targeted path. The path of the sports car is the best matching the targeted paths. This is proven by the RMS values of 0021 and 0.0927 (Table 6). At 120 km/h, the best vehicle is the sedan since its RMS value is 0.8711. According to the table, the best performance for DLC is at the lowest speed of 80 km/h since its RMS is the lowest in average for all vehicles. This is logically right. At low speed, the lateral acceleration is low. Therefore, it produces low lateral force and low lateral motion, and eventually, the vehicle can follow the targeted path. In terms of the weight of the vehicle, the lightest vehicle performed the best in DLC test. Low weight means low lateral force at easier for the vehicle to counter lateral motion to follow the targeted path. Additionally, the lowest COG of the vehicle is the best is following the targeted path. This is due to the roll moment. At low COG, the roll moment is low. Therefore, low moment compensation is needed to follow the path.
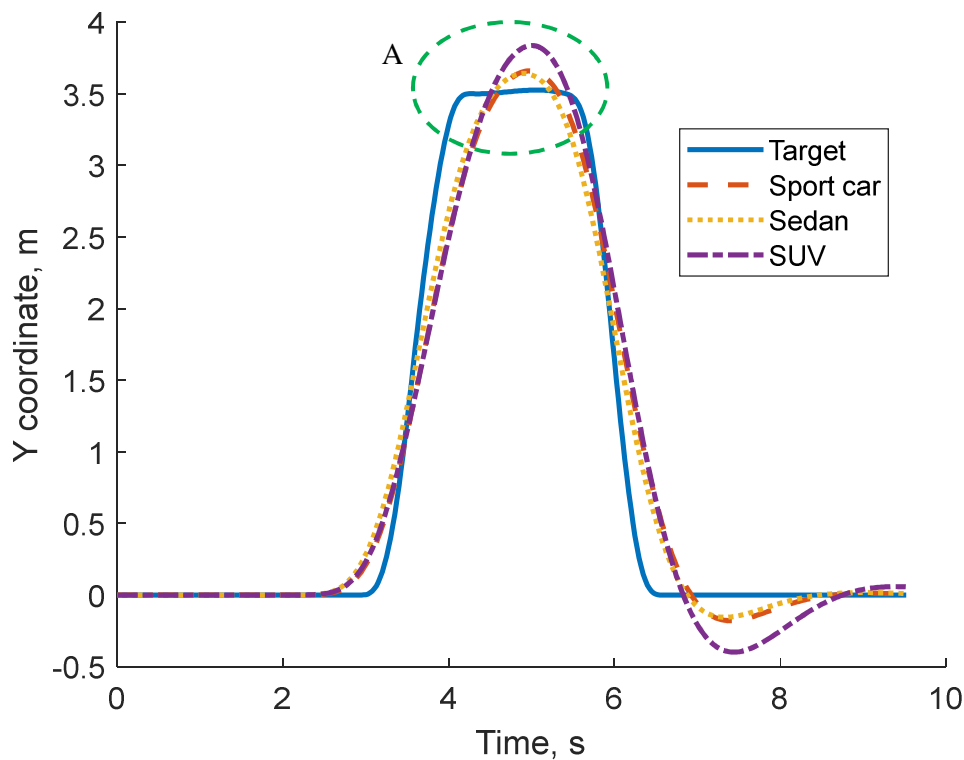
Figure 21: *Y* coordinate of all vehicles compared to target at 80 km/h

Tabel 6: RMS values comparison between the vehicle *y*-coordinate and target

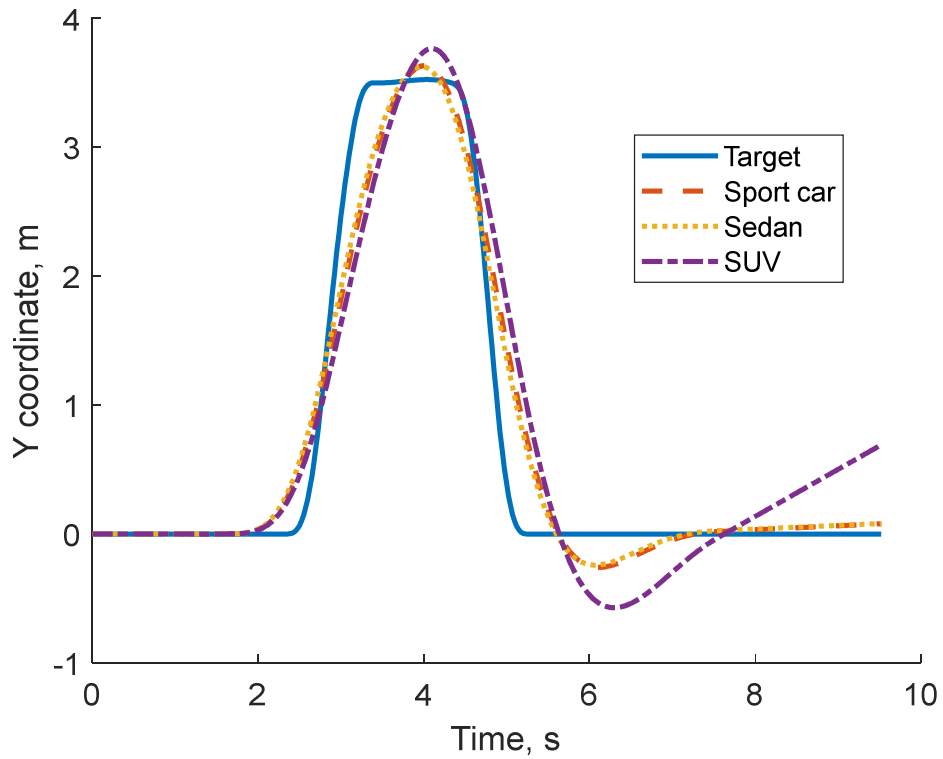| Speed (km/h)			80	100	120
Vehicle	Weight (kg)	COG (m)	RMS		
Sport car	1360	0.375	0.0021	0.0927	0.8818
Sedan	1650	0.530	0.0026	0.0946	0.8711
SUV	2257	0.781	0.0507	0.8651	2.0110

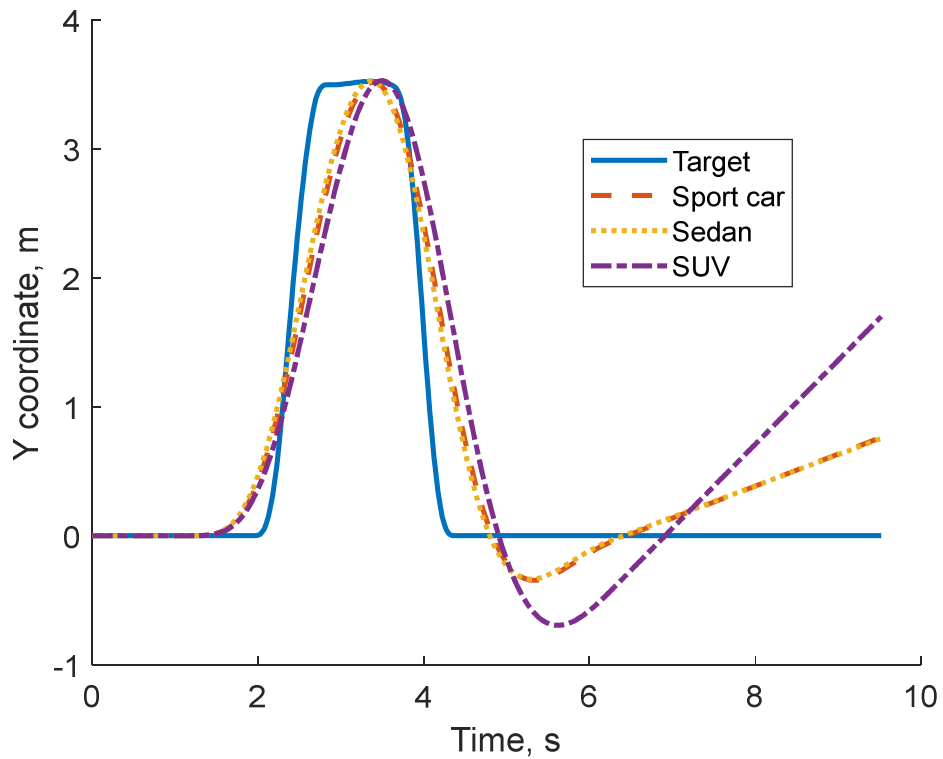Figure 22: *Y* coordinate of all vehicles compared to target at 100 km/h

Figure 23: *Y* coordinate of all vehicles compared to target at 120 km/h

4.0   CONCLUSION

The common models in analyzing the tire behaviours in terms of longitudinal and lateral forces have been studied. The Simulink models of the Magic, Calspan, and Dugoff tire models have been developed. The models have been verified by the simulation results of three different vehicles at three different speeds through DLC test. It can be concluded that the best DLC test is performed at low speed and the best tire model is the Calspan tire model. In term of vehicle, the lower the COG and weight, the better the performance of the vehicle. The Simulink models of the tires can be used for further analysis on longitudinal and lateral dynamic control of a vehicle. Based on the results and observations, with the same tire size, the performance of different vehicles can be studied and analyzed.

5.0   ACKNOWLEDGEMENT

6.0   REFERENCES

[1]   Benekohal, R. F., & Treiterer, J. (1988). CARSIM: Car-following model for simulation of traffic in normal and stop-and-go conditions. *Transportation research record*, *1194*, 99-111.

[2]   Dupuy, S., Egges, A., Legendre, V., & Nugues, P. (2001). Generating a 3D simulation of a car accident from a written description in natural language: The Carsim system. *arXiv preprint cs/0105023*.

[3]   Kinjawadekar, T., Dixit, N., Heydinger, G. J., Guenther, D. A., & Salaani, M. K. (2009). *Vehicle dynamics modeling and validation of the 2003 Ford Expedition with ESC using CarSim* (No. 2009-01-0452). SAE Technical Paper.

[4]   Åkerberg, O., Svensson, H., Schulz, B., & Nugues, P. (2003). CarSim: an automatic 3D text-to-scene conversion system applied to road accident reports. In *Demonstrations*.

[5]   Johansson, R., Williams, D., Berglund, A., & Nugues, P. (2004, July). Carsim: a system to visualize written road accident reports as animated 3d scenes. In *Proceedings of the 2nd Workshop on Text Meaning and Interpretation* (pp. 57-64).

[6]   Li, Y., Deng, H., Xu, X., & Wang, W. (2018). Modelling and testing of in-wheel motor drive intelligent electric vehicles based on co-simulation with Carsim/Simulink. *IET Intelligent Transport Systems*, *13*(1), 115-123.

[7]   Kinjawadekar, T. (2009). *Model-based Design of an Electronic Stability Control System for Passenger Cars Using CarSim and Matlab-Simulink* (Doctoral dissertation, The Ohio State University).

[8]   Etienne, L., Lúa, C. A., Di Gennaro, S., & Barbot, J. P. (2020). A super-twisting controller for active control of ground vehicles with lateral tire-road friction estimation and CarSim validation. *International Journal of Control, Automation and Systems*, *18*(5), 1177-1189.

[9]   Konghui, G., Hao, F., Haitao, D., Dang, L., & Lingge, J. (2008). Development of controller for vehicle stability system based on CarSim RT [J]. *Automobile Technology*, *3*.

[10]   Khalili, E., Ghaisari, J., & Danesh, M. (2017, November). Control and analysis of the vehicle motion using sliding mode controller and Carsim software. In *2017 5th International Conference on Control, Instrumentation, and Automation (ICCIA)* (pp. 1-5). IEEE.

[11]   Zhu, M. T., Shao, C. Z., & Wang, G. L. (2010). Research on road model rebuilding and vehicle simulation of ride comfort based on carsim software [J]. *Machinery Design & Manufacture*, *10*, 78-80.

[12]   Egges, A., Nijholt, A., & Nugues, P. (2001). Generating a 3D Simulation of a Car Accident from a Formal Description: the CarSim System.

[13]   Zhao, S., & Zhu, L. (2018). Cruise Control System Based on Joint Simulation of CarSim and Simulink. *Open Access Library Journal*, *5*(7), 1-8.

[14]   Liu, J., Zhang, L., Xiao, S., & Xin, X. (2014, July). Development of virtual drive HILS system based on VR and CarSim. In *Proceedings of the 33rd Chinese Control Conference* (pp. 6441-6444). IEEE.

[15]   Ji, F. Z., Zhou, X. X., & Zhu, W. B. (2014). Coordinate control of electro-hydraulic hybrid brake of electric vehicles based on CarSim. In *Applied Mechanics and Materials* (Vol. 490, pp. 1120-1125). Trans Tech Publications Ltd.

[16]   Dumitriu, D. N., Chiroiu, V., & Munteanu, L. (2015). Car vertical dynamics simulations using both an in-house 7 DOF model simulator and Carsim commercial software. *UPB Scientific Bulletin, Series D: Mechanical Engineering*, *77*(1), 77-84.

[17]   SUN, Y. K., & FAN, X. B. (2017). Research on the application of CarSim in vehicle simulation and development. *International Journal*, *4*.

[18]   Abdullah, M. A., Jamil, J. F., & Salim, M. A. (2015, November). Dynamic performances analysis of a real vehicle driving. In *IOP Conference Series: Materials Science and Engineering* (Vol. 100, No. 1, p. 012017). IOP Publishing.

[19]   Abdullah, M. A., & Rahim, M. A. (2016). Driving behaviour analysis of young vehicle drivers. *Proceedings of Mechanical Engineering Research Day*, *2016*, 19-20.

[20]   Abdullah, M. A., Jamil, J. F., & Mohan, A. E. (2016). Vehicle dynamics modeling & simulation. *Centre for Advanced Research on Energy (CARe), Faculty of Mechanical Engineering, Universiti Teknikal Malaysia Melaka*, *2016*.

[21]   Abdullah, M. A., Ibrahim, M., & Abdul Rahim, M. A. H. (2017). Experimental and analysis of vehicle dynamics performance based on driving behavior. *Journal of Mechanical Engineering (JMechE)*, (1), 193-206.

[22]   Abdullah, M. A., Jamil, J. F., Yamin, A. M., Nuri, N. M., & Hassan, M. Z. (2015). Vehicle Dynamics. *Teaching and Learning Series, Faculty of Mechanical Engineering, Module*, *10*.

[23]   Abdullah, M. A., Salim, M. A., & Nasir, M. M. (2014). *Dynamics performances of Malaysian passenger vehicle*. ARPN Journal of Engineering and Applied Sciences 10 (17), 7759-7763.

[24]   Zhang, H., Zhang, X., & Wang, J. (2014). Robust gain-scheduling energy-to-peak control of vehicle lateral dynamics stabilisation. *Vehicle System Dynamics*, *52*(3), 309-340.

[25]   Sierra, C., Tseng, E., Jain, A., & Peng, H. (2006). Cornering stiffness estimation based on vehicle lateral dynamics. *Vehicle System Dynamics*, *44*(sup1), 24-38.

[26]   Zhang, H., & Wang, J. (2015). Vehicle lateral dynamics control through AFS/DYC and robust gain-scheduling approach. *IEEE Transactions on Vehicular Technology*, *65*(1), 489-494.

[27] Oudghiri, M., Chadli, M., & El Hajjaji, A. (2008). Robust observer-based fault-tolerant control for vehicle lateral dynamics. *International Journal of vehicle design*, *48*(3-4), 173-189.

[28] Du, H., Zhang, N., & Naghdy, F. (2011). Velocity-dependent robust control for improving vehicle lateral dynamics. *Transportation research part C: emerging technologies*, *19*(3), 454-468.

[29] Du, H., Zhang, N., & Dong, G. (2010). Stabilizing vehicle lateral dynamics with considerations of parameter uncertainties and control saturation through robust yaw control. *IEEE Transactions on Vehicular Technology*, *59*(5), 2593-2597.

[30] Mammar, S., Glaser, S., & Netto, M. (2006, June). Vehicle lateral dynamics estimation using unknown input proportional-integral observers. In *2006 American control conference* (pp. 6-pp). IEEE.

[31] El Hajjaji, A., Chadli, M., Oudghiri, M., & Pages, O. (2006, June). Observer-based robust fuzzy control for vehicle lateral dynamics. In *2006 American Control Conference* (pp. 6-pp). IEEE.

[32] Liaw, D. C., Chiang, H. H., & Lee, T. T. (2007). Elucidating vehicle lateral dynamics using a bifurcation analysis. *IEEE Transactions on Intelligent Transportation Systems*, *8*(2), 195-207.

[33] Huang, Y., Liang, W., & Chen, Y. (2021). Stability Regions of Vehicle Lateral Dynamics: Estimation and Analysis. *Journal of Dynamic Systems, Measurement, and Control*, *143*(5).

[34] Sakthivel, R., Mohanapriya, S., Ahn, C. K., & Selvaraj, P. (2018). State estimation and dissipative-based control design for vehicle lateral dynamics with probabilistic faults. *IEEE Transactions on Industrial Electronics*, *65*(9), 7193-7201.

[35] Su, J., & Chen, W. H. (2016, March). Fault diagnosis for vehicle lateral dynamics with robust threshold. In *2016 IEEE International Conference on Industrial Technology (ICIT)* (pp. 1777-1782). IEEE.

[36] Su, J., & Chen, W. H. (2016, March). Fault diagnosis for vehicle lateral dynamics with robust threshold. In *2016 IEEE International Conference on Industrial Technology (ICIT)* (pp. 1777-1782). IEEE.

[37] Jin, X., Yin, G., Li, Y., & Li, J. (2016). Stabilizing vehicle lateral dynamics with considerations of state delay of AFS for electric vehicles via robust gain-scheduling control. *Asian Journal of Control*, *18*(1), 89-97.

[38] Jin, X., Yin, G., Li, Y., & Li, J. (2016). Stabilizing vehicle lateral dynamics with considerations of state delay of AFS for electric vehicles via robust gain-scheduling control. *Asian Journal of Control*, *18*(1), 89-97.

[39] Farrelly, J., & Wellstead, P. (1996, September). Estimation of vehicle lateral velocity. In *Proceeding of the 1996 IEEE International Conference on Control Applications IEEE International Conference on Control Applications held together with IEEE International Symposium on Intelligent Contro* (pp. 552-557). IEEE.

[40] Peng, H. (1993). Vehicle lateral control for highway automation.

[41] Mohanapriya, S., Sakthivel, R., & Almakhles, D. J. (2020). Repetitive control design for vehicle lateral dynamics with state-delay. *IET Control Theory & Applications*, *14*(12), 1619-1627.

[42] Varrier, S., Koenig, D., & Martinez, J. J. (2012, December). Robust fault detection for vehicle lateral dynamics. In *2012 IEEE 51st IEEE Conference on Decision and Control (CDC)* (pp. 4366-4371). IEEE.

[43] Kuiper, E. V. O. J., & Van Oosten, J. J. M. (2007). The PAC2002 advanced handling tire model. *Vehicle system dynamics*, *45*(S1), 153-167.

[44] Tezuka, Y., Ishii, H., & Kiyota, S. (2001). Application of the magic formula tire model to motorcycle maneuverability analysis. *JSAE review*, *22*(3), 305-310.

[45]   Mashadi, B., Mousavi, H., & Montazeri, M. (2015). Obtaining relations between the Magic Formula coefficients and tire physical properties. *International Journal of Automotive Engineering*, *1*, 911-922.

[46]   Mizuno, M. (2003). Development of tire side force model based on magic formula with the influence of tire surface temperature. *R&D Review of Toyota CRDL*, *38*(4), 17-22.

[47]   Cabrera, J. A., Castillo, J. J., Pérez, J., Velasco, J. M., Guerra, A. J., & Hernández, P. (2018). A procedure for determining tire-road friction characteristics using a modification of the magic formula based on experimental results. *Sensors*, *18*(3), 896.

[48]   Pacejka, H. B., & Bakker, E. (1992). The magic formula tyre model. *Vehicle system dynamics*, *21*(S1), 1-18.

[49]   Boyle, S. (2019, December). Pacejka Magic Formula Tire Model Parser. In *2019 International Conference on Computational Science and Computational Intelligence (CSCI)* (pp. 517-518). IEEE.

[50]   Li, B., Yang, X., & Yang, J. (2014). Tire model application and parameter identification-a literature review. *SAE International Journal of Passenger Cars-Mechanical Systems*, *7*(2014-01-0872), 231-243.

[51]   Guang-sheng, R. E. N. (2001). Optimization of Curve Fitting Used in Development of Magic Formula Tire Model [J]. *Journal of Chongqing University (Natural Science Edition)*, *3*.

[52]   Salaani, M. K., Heydinger, G. J., & Grygier, P. A. (2006). Measurement and Modeling of Tire Forces on a Low Coefficient Surface. *SAE Transactions*, 392-399.

[53]   Allen, R. W., Magdaleno, R. E., Rosenthal, T. J., Klyde, D. H., & Hogue, J. R. (1995). Tire modeling requirements for vehicle dynamics simulation. *SAE transactions*, 484-504.

[54]   Kasprzak, E. M., & Gentz, D. (2006). *The formula sae tire test consortium-tire testing and data handling* (No. 2006-01-3606). SAE Technical Paper.

[55]   Kasprzak, E. M., Lewis, K. E., & Milliken, D. L. (2006). Inflation pressure effects in the nondimensional tire model. *SAE Transactions*, 1781-1792.

[56]   Sayers, M. W., & Han, D. (1996). A generic multibody vehicle model for simulating handling and braking. *Vehicle system dynamics*, *25*(S1), 599-613.

[57]   Sadeghi, S., & Ahmadian, M. T. (2001). Tire Modeling with Nonlinear Behavior for Vehicle Dynamic Studies.

[58]   Nasir, M. Z. M., Hudha, K., Amir, M. Z., & Kadir, F. A. A. (2012). Modelling, simulation and validation of 9 DOF vehicles model for automatic steering system. In *Applied Mechanics and Materials* (Vol. 165, pp. 192-196). Trans Tech Publications Ltd.

[59]   Allen, R. W., Rosenthal, T. J., & Chrstos, J. P. (1997). *A vehicle dynamics tire model for both pavement and off-road conditions* (No. 970559). SAE Technical Paper.

[60]   Bergman, W., & Clemett, H. R. (1975). Tire cornering properties. *Tire Science and Technology*, *3*(3), 135-163.

[61]   Ding, N., & Taheri, S. (2010). A modified Dugoff tire model for combined-slip forces. *Tire Science and Technology*, *38*(3), 228-244.

[62]   Chen, L., Bian, M., Luo, Y., & Li, K. (2013, July). Maximum tire road friction estimation based on modified Dugoff tire model. In *2013 international conference on mechanical and automation engineering* (pp. 56-61). IEEE.

[63]   Bian, M., Chen, L., Luo, Y., & Li, K. (2014). *A dynamic model for tire/road friction estimation under combined longitudinal/lateral slip situation* (No. 2014-01-0123). SAE Technical Paper.

[64]   Song, S., Chun, M. C. K., Huissoon, J., & Waslander, S. L. (2014, June). Pneumatic trail based slip angle observer with Dugoff tire model. In *2014 IEEE Intelligent Vehicles Symposium Proceedings* (pp. 1127-1132). IEEE.

[65]   Chen, L., Bian, M., Luo, Y., & Li, K. (2015). *Estimation of road-tire friction with unscented Kalman filter and MSE-weighted fusion based on a modified Dugoff tire model* (No. 2015-01-1601). SAE Technical Paper.

[66]   He, R., Jimenez, E., Savitski, D., Sandu, C., & Ivanov, V. (2016). Investigating the parameterization of Dugoff tire model using experimental tire-ice data. *SAE International Journal of Passenger Cars-Mechanical Systems*, *10*(2016-01-8039), 83-92.

[67]   Dugoff, H., Fancher, P. S., & Segel, L. (1970). An analysis of tire traction properties and their influence on vehicle dynamic performance. *SAE transactions*, 1219-1243.
[68]   ZHOU, L., & ZHANG, X. W. (2012). Simulation of Vehicle Dynamics in Tire Blow-out Process Based on Dugoff Tire Model [J]. *Computer Simulation*, *6*.

[69]   Villagra, J., D'Andréa-Novel, B., Fliess, M., & Mounier, H. (2011). A diagnosis-based approach for tire–road forces and maximum friction estimation. *Control engineering practice*, *19*(2), 174-184.

[70]   Bhoraskar, A., & Sakthivel, P. (2017, January). A review and a comparison of Dugoff and modified Dugoff formula with Magic formula. In *2017 International Conference on Nascent Technologies in Engineering (ICNTE)* (pp. 1-4). IEEE.

[71] Kissai, M., Monsuez, B., Tapus, A., & Martinez, D. (2017, September). A new linear tire model with varying parameters. In *2017 2nd IEEE International Conference on Intelligent Transportation Engineering (ICITE)* (pp. 108-115). IEEE.

[72] Han, K. S., Lee, E., & Choi, S. (2015, October). Estimation of the maximum lateral tire-road friction coefficient using the 6-DoF sensor. In *2015 15th International Conference on Control, Automation and Systems (ICCAS)* (pp. 1734-1738). IEEE.

[73] Jin, X., Yin, G., & Lin, Y. (2014). *Interacting multiple model filter-based estimation of lateral tire-road forces for electric vehicles* (No. 2014-01-2321). SAE Technical Paper.

[74] ISO 3888-2:2011, Passenger cars - Test track for a severe lane-change manoeuvre - Part 2: Obstacle avoidance.

[75] Peng, Y., & Yang, X. (2012). Comparison of various double-lane change manoeuvre specifications. *Vehicle system dynamics*, *50*(7), 1157-1171.

[76] Lee, J., & Chang, H. J. (2018). Explicit model predictive control for linear time-variant systems with application to double-lane-change maneuver. *Plos one*, *13*(12), e0208071.

[77] Katzourakis, D., de Winter, J. C., de Groot, S., & Happee, R. (2012). Driving simulator parameterization using double-lane change steering metrics as recorded on five modern cars. *Simulation Modelling Practice and Theory*, *26*, 96-112.

[78] El Hajjaji, A., & Ouladsine, M. (2001, September). Modeling human vehicle driving by fuzzy logic for standardized ISO double lane change maneuver. In *Proceedings 10th IEEE International Workshop on Robot and Human Interactive Communication. ROMAN 2001 (Cat. No. 01TH8591)* (pp. 499-503). IEEE.

[79] Arefnezhad, S., Ghaffari, A., Khodayari, A., & Nosoudi, S. (2018). Modeling of double lane change maneuver of vehicles. *International Journal of Automotive Technology*, *19*(2), 271-279.

[80] Hatipoglu, C., Ozguner, U., & Redmill, K. A. (2003). Automated lane change controller design. *IEEE transactions on intelligent transportation systems*, *4*(1), 13-22.

[81] Huang, C., Naghdy, F., & Du, H. (2016, November). Model predictive control-based lane change control system for an autonomous vehicle. In *2016 IEEE Region 10 Conference (TENCON)* (pp. 3349-3354). IEEE.

[82] Kutluay, E., & Winner, H. (2012, December). Assessment methodology for validation of vehicle dynamics simulations using double lane change maneuver. In *Proceedings of the 2012 Winter Simulation Conference (WSC)* (pp. 1-12). IEEE.

[83] Naude, A. F., & Steyn, J. L. (1993). *Objective evaluation of the simulated handling characteristics of a vehicle in a double lane change manoeuvre* (No. 930826). SAE Technical Paper.

[84] Sledge Jr, N. H., & Marshek, K. M. (1997). Comparison of ideal vehicle lane-change trajectories. *SAE transactions*, 2004-2027.

[85] Hess, D., & Sattel, T. (2011, October). Double-lane change optimization for a stochastic vehicle model subject to collision probability constraints. In *2011 14th International IEEE Conference on Intelligent Transportation Systems (ITSC)* (pp. 206-211). IEEE.

[86] Yang, X., & Gander, J. (2011). Driver's Preview Strategy and its Impact on NATO Double Lane Change Maneuver. *SAE International Journal of Materials and Manufacturing*, *4*(1), 1025-1035.

[87] Forkenbrock, G. J., Garrott, W. R., Heitz, M., & O'Harra, B. C. (2003). An experimental examination of double lane change maneuvers that may induce on-road, untripped, light vehicle rollover. *SAE transactions*, 1128-1144.

[88] Angelis, S., Tidlund, M., Leledakis, A., Lidberg, M., Nybacka, M., & Katzourakis, D. (2014). Optimal steering for double-lane change entry speed maximization. In *ACEV'14 International symposium on advanced vehicle control, 22-26 September 2014, Tokyo, Japan*. Society of Automotive Engineers.

[89] Willmott, C. J., & Matsuura, K. (2005). Advantages of the mean absolute error (MAE) over the root mean square error (RMSE) in assessing average model performance. *Climate research*, *30*(1), 79-82.

[90] Chai, T., & Draxler, R. R. (2014). Root mean square error (RMSE) or mean absolute error (MAE). *Geoscientific Model Development Discussions*, *7*(1), 1525-1534.

[91] Chai, T., & Draxler, R. R. (2014). Root mean square error (RMSE) or mean absolute error (MAE)?–Arguments against avoiding RMSE in the literature. *Geoscientific model development*, *7*(3), 1247-1250.

[92] Maiorov, V. N., & Crippen, G. M. (1994). Significance of root-mean-square deviation in comparing three-dimensional structures of globular proteins. *Journal of molecular biology*, *235*(2), 625-634.

[93] Salmon, T. O., & van de Pol, C. (2006). Normal-eye Zernike coefficients and root-mean-square wavefront errors. *Journal of Cataract & Refractive Surgery*, *32*(12), 2064-2074.

[94] Applegate, R. A., Ballentine, C., Gross, H., Sarver, E. J., & Sarver, C. A. (2003). Visual acuity as a function of Zernike mode and level of root mean square error. *Optometry and Vision Science*, *80*(2), 97-105.

[95] Huffman, G. J. (1997). Estimates of root-mean-square random error for finite samples of estimated precipitation. *Journal of Applied Meteorology*, *36*(9), 1191-1201.

[96] Hespanha, J. P. (2003). Root-mean-square gains of switched linear systems. *IEEE Transactions on Automatic Control*, *48*(11), 2040-2045.

[97] DiStefano, C., Liu, J., Jiang, N., & Shi, D. (2018). Examination of the weighted root mean square residual: Evidence for trustworthiness?. *Structural Equation Modeling: A Multidisciplinary Journal*, *25*(3), 453-466.

[98] O'Donovan, T. S., & Murray, D. B. (2007). Jet impingement heat transfer–Part I: Mean and root-mean-square heat transfer and velocity distributions. *International journal of heat and mass transfer*, *50*(17-18), 3291-3301.

[99] Szostack, H. T., Allen, R. W., & Rosenthal, T. J. (1988). Analytical modeling of driver response in crash avoidance maneuvering. Volume 2: an interactive tire model for driver/vehicle simulation (No. STI-TR-1227-1-V2).